Role of heparan sulfate in vasculogenesis of dental pulp stem cells

Osaka University Graduate School of Dentistry

Oral Science Course

Department of Dental Biomaterials

Supervisor: Professor Satoshi Imazato

Aonan Li

Acknowledgment

During the past four-year Ph.D. journey at Osaka University since 2019, I have received innumerable assistance and support from many, many people.

I would like to express my deepest gratitude to my mentor, Professor Satoshi Imazato, Chair of the Department of Dental Biomaterials, Osaka University Graduate School of Dentistry, for accepting me and giving me this opportunity to study abroad and gain research experience. He is such a knowledgeable and warm person, who always generously encouraged and motivated me. I learned a lot from him, not only in the field of scientific research but also about his life attitude. I am so grateful to have such an intelligent and approachable mentor during these four years.

I would like to give many thanks to my supervisor Associate Professor, Jun-Ichi Sasaki for consistently providing me with invaluable advice and tremendous support. Thank you so much for always offering me brilliant hints and helping me expand my thinking, along with patience and kindness. Without his kind assistance and encouragement, I could not be the person I am today. His rigorous working attitude will benefit me throughout my life.

I would also like to acknowledge all the teachers and members of our

department, thank you for creating a comfortable and energetic academic environment. You have made my life in Japan more enjoyable, and I will always cherish the wonderful moments we shared together.

To my parents, thank you for always supporting me unconditionally, no matter what decisions I have made. I hope I can make you proud of me with my academic achievements and contributions to science.

To my beloved husband, best friend, and family, Li Jiannan, your selfless love, comfort, and accompany are the source of my confidence and driving force to overcome obstacles. I consider myself fortunate to have met you and I am prepared to spend the rest of my life with you, whatever happens.

Finally, I appreciate the Chinese Scholarship Council, which financially supported me in Japan.

Aonan Li

INDEX

Introduction

Recovery from ischemic injury and survival of engineered tissues after implantation rely on a stable blood supply and functional vasculature formation [1,2]. Vascular endothelial cells line the inner surface of blood vessels, which are stabilized by the surrounding basement membrane and pericytes [3,4]. With the exception of a few poorly vascularized tissue such as the cornea and skin epidermis, most metabolically active tissues can only reside within 200 μm of the capillary network since the nutrient supply and oxygen diffusion through tissues is limited to this distance, unveiling the indispensable role of vasculature formation [5,6].

Throughout the process of blood vessel generation, neovascularization plays a fundamental role in creating primitive vascular networks and subsequent blood perfusion by the host vasculature [7,8]. Vasculogenesis, which refers to the assembling of stem cells and endothelial progenitor cells into endothelium and subsequent formation of nascent capillaries, contributes to adult neovascularization [9,10]. Therefore, elucidation of vasculogenesis of stem cells will facilitate control of neovascularization and further development of novel tissue regenerative therapies.

Dental pulp stem cells (DPSCs), which are classified as mesenchymal stem cells (MSCs), are highly proliferative and exhibit multipotent differentiation into osteoblasts, chondrocytes, and adipocytes [11–13]. Notably, owing to the constitutive expression of vascular endothelial growth factor (VEGF) receptor 1, DPSCs more readily differentiate into vascular endothelial lineages compared with other mesenchymal cells derived from bone marrow and adipose tissues [14–16]. The excellent vasculogenic capacity of DPSCs is of great interest when considering stem cell therapy involving dental pulp regeneration and/or vascular regenerative medicine [17–19]. Recent research demonstrated that canonical Wnt/β-catenin and p53/p21 signaling are required for vasculogenic differentiation of DPSCs [20,21]. In addition, phosphorylation of mitogen-activated protein kinase kinase 1 (MEK1)/extracellular signal-regulated kinase (ERK) and downstream E-26 transformation-specific-related gene (ERG) activation lead to vascular endothelial (VE)-cadherin expression, which is highly involved in the capillary sprouting of DPSCs and further anastomosis with the host vasculature [22]. To date, focus has been placed on signaling pathways and molecular regulation of vasculogenic processes in DPSCs, with limited knowledge concerning the roles of the extracellular microenvironment.

Extracellular matrix (ECM) is the non-cellular three-dimensional (3D) network structure present within all tissues and organs, surrounding cells with a complex combination of proteoglycans, growth factors, and cytokines [23,24]. ECM provides not only structural integrity and support for cell survival, but it can also determine cell behaviors by interacting with cells under physiological and pathological conditions [25–29]. Temporal and spatial control of ECM remodeling during blood vessel formation enables changes in matrix deposition and degradation, which in turn trigger cell migration and differentiation by releasing angiogenic factors [30,31]. This subsequently contributes to the development of nascent capillaries and vascular homeostasis. ECM-based biological materials have been effectively applied for regeneration and reconstruction of ischemic tissues [32–37].

Proteoglycans are widely distributed constituents of ECM in all mammalian tissues, which are composed of glycosaminoglycan chains and covalently core protein [38,39]. Based on the sulfation site and disaccharide structure, glycosaminoglycans are classified into four groups; chondroitin sulfate, keratin sulfate, hyaluronan, and heparan sulfate (HS) [40,41]. In particular, it is considered that HS is more influential in regulating cellular functions than other

types of proteoglycans, in part because of the structural complexity of HS chains exhibiting various sulfation patterns and conformational flexibility [40,42]. HS could enhance the binding affinity between growth factors and related receptors to modulate a variety of biological activities, including vascular formation and tumor progression [43–45]. It was demonstrated that proliferation and angiogenesis of VEGF-stimulated endothelial cell were dependent on HS, which is also highly involved in the vascular permeability of blood vessels [46,47]. Furthermore, recent studies revealed that HS together with basic fibroblast growth factor (bFGF) promoted ischemic heart repair after myocardial infarction, and HS-bound $VEGF_{165}$ enhanced functional recovery from cerebral ischemia [48,49]. One of the earliest studies of HS showed that HS proteoglycans were required for hematopoietic lineage differentiation, indicating a possible relationship between HS and vasculogenic development [50]. In addition, HS has been implicated in the differentiation of embryonic stem cells into endothelial cells *in vitro* in mice embryoid bodies, which was further supported by an *in vivo* zebrafish embryo model [51]. Despite these intriguing results obtained using embryonic models, little is known about the role of HS in endothelial differentiation and neovascularization of mesenchymal cells.

In this study, it was hypothesized that HS highly orchestrates endothelial differentiation of DPSCs and their subsequent formation of nascent blood vessels. To explore vasculogenic behaviors in DPSCs under HS deficiency, an HS antagonist, surfen molecule [52], and silencing of *exostosin 1* (*EXT1*), which exerts a key function in regulating the initial process of HS biosynthesis [53], were utilized. Moreover, the role of HS in vascular formation was investigated by transplanting *EXT1*-silenced DPSCs into mice. The purpose of this study is to elucidate the role of HS in endothelial differentiation and vasculogenesis of DPSCs in detail.

Chapter 1: Vasculogenic behaviors of HS antagonist-treated DPSCs

Objectives

- To assess DPSC proliferative and sprouting ability under exposure to the HS antagonist (surfen).
- To evaluate the devitalization and revitalization of sprouting capacity of surfen-exposed DPSCs.
- To determine endothelial and stemness-related gene expressions in surfen treated DPSCs.

1. Materials and methods

1.1 HS antagonist

Surfen hydrate (bis-2-methyl-4-amino-quinolyl-6-carbamide) powder was purchased from Sigma-Aldrich (MO, USA). The stock solution at 10 mM was prepared with dimethyl sulfoxide (Nacalai Tesque, Kyoto, Japan) and stored in the glass container at -20°C without light. The indicated working solutions at different concentrations of surfen were prepared freshly as needed.

1.2 Cell culture

DPSCs isolated from human adult third molars (Lonza, Basel, Switzerland) were cultured in Dulbecco's Modified Eagle's Medium (DMEM; Wako, Osaka, Japan) containing 20% fetal bovine serum (Thermo Fisher Scientific, MA, USA) and 1% penicillin/streptomycin (Sigma-Aldrich), which was designated as growth medium (GM). To induce endothelial differentiation, DPSCs were cultured in an endothelial differentiation medium (EM) consisting of EGM2-MV (Lonza) supplemented with 50 ng/mL rhVEGF$_{165}$ (R&D Systems, MN, USA). Cells were incubated in a humidified atmosphere at 37°C with 5% CO_2.

1.3 HS production

DPSCs at an initial density of 500 cells/cm^2 were cultured in GM or EM containing different concentrations (1, 5, 10 μM) of surfen for 7 days. Subsequently, cells were washed twice with phosphate-buffered saline (PBS; Gibco, NY, USA), and treated with ice-cold RIPA lysis buffer (Santa Cruz Biotechnology, CA, USA) for 10 min on ice. Cell lysate was collected by the disposable cell scraper and transferred to a 1.5 mL Eppendorf tube, followed by centrifuging at 13,000 rpm

for 10 min at 4°C. Supernatant was then transferred to another 1.5 mL tube, and HS production by DPSCs was quantified using the enzyme-linked immunosorbent assay (ELISA) kit (MyBioSource, San Diego, USA) for general HS, based on the principle of enzyme-substrate reaction, according to the manufacturer's instructions. Immunoenzymatic detection at a 450 nm wavelength was measured by the iMark microplate reader (Bio-Rad, CA, USA). The experiments were repeated four times. The data of HS production with surfen treatment were analyzed by the one-way analysis of variance (ANOVA) and Tukey's Honestly Significant Difference (HSD) test with a significance level of $P < 0.05$.

1.4 Cell proliferation

The proliferative ability of surfen-exposed DPSCs was evaluated using a water-soluble tetrazolium-8 (WST-8) assay kit (Dojindo, Tokyo, Japan), based on the mechanism that tetrazolium salt is cleaved into formazan dye by the metabolic activity of living cells. The amount of formazan dye directly correlates with the number of live cells.

DPSCs were seeded in 96-well culture plates at a density of 500 cells/well

to allow attachment overnight. The following day, cells were cultured with 100 μL of GM or EM containing 1, 5, or 10 μM surfen. After culturing for 1, 3, or 5 days, 10 μL of WST-8 solution was added to each well, and plates were incubated for an additional 2 h. The absorbance at 450 nm of each well was measured using the iMark microplate reader (Bio-Rad). Additionally, the cell morphologies under different treatments at each time point were observed by a light microscope (CK40-F100; Olympus, Tokyo, Japan) equipped with a CCD camera. The experiments were repeated four times. Relative cell numbers among all groups were analyzed by the one-way ANOVA and Tukey's HSD test with a significance level of $P < 0.05$.

1.5 Vascular sprouting

A capillary-sprouting assay was carried out to quantify the sprouting ability and reticular structure formation of DPSCs in three-dimensional (3D) culture, according to a previous study [22]. First, 300 μL of Growth Factor-Reduced Matrigel (Corning, NY, USA) was poured into 24-well culture plates and polymerized at 37°C for 1 h. Then, 1×10^4 DPSCs were seeded onto Matrigel-precoated plates and maintained in 1 mL of EM in the absence or presence of 1,

5, or 10 μM of surfen. After incubation for 1, 3, 7, and 14 days, images were captured with the light microscope (CK40-F100) equipped with a CCD camera. Four independent images from different views of each group were randomly selected for further analysis.

Numbers and total length of branches were measured using ImageJ software (National Institutes of Health, MD, USA). The images were imported into the software and examined by the “Angiogenesis Analyzer” plug-in. The processed images were then created by clicking the “Analyze HUVEC Phase Contrast”. The data were statistically analyzed by utilizing the one-way ANOVA and Tukey’s HSD test with a significance level of $P < 0.05$.

1.6 Devitalization and revitalization

To evaluate the devitalization and revitalization of sprouting ability upon surfen exposure, 1×10^4 DPSCs were seeded onto Matrigel-precoated 24-well culture plates and divided into four groups. Devitalization of DPSC sprouting ability was evaluated in groups 1 (G1) and 2 (G2), while revitalization was evaluated in groups 3 (G3) and 4 (G4). The detailed information of each group were as follows; G1: DPSCs were maintained in EM for the first 7 days, followed by EM containing

5 μM surfen for another 7 days. G2: DPSCs were maintained in EM for the first 7 days, followed by EM containing 10 μM surfen for another 7 days. G3: DPSCs were cultured in EM containing 5 μM surfen for the first 7 days, followed by EM without surfen for another 7 days. G4: DPSCs were cultured in EM containing 10 μM surfen for the first 7 days, followed by 1 mL of EM for another 7 days.

At the indicated time points, images were captured using the light microscope (CK40-F100), and numbers and total lengths of branches were determined by the ImageJ software, as described above. Four independent images from different views of each group were randomly selected for statistical analysis. The statistical data were analyzed by the one-way ANOVA and Tukey's HSD test with a significance level of $P < 0.05$.

1.7 Cell viability

Live/dead staining was performed to assess cell viability in 3D cultures. Briefly, 1×10^4 DPSCs were seeded onto Matrigel-precoated 24-well culture plates in EM with surfen at concentrations of 1, 5, or 10 μM. DPSCs cultured without surfen were used as a control. After 7 or 14 days, cells were stained with a LIVE/DEAD Viability/Cytotoxicity Kit (Thermo Fisher Scientific) according to the

manufacturer's instructions. The cells were gently washed with PBS twice, and then living cells were stained with the 2 μM of esterase substrate calcein AM working solution, whereas dead cells were stained with 4 μM of membrane-impermeable DNA-binding dye ethidium homodimer 1. After incubating the cells for 20 min at room temperature, stained areas were observed with a fluorescent microscope (TE2000) at 475 nm and 559 nm for living cells and dead cells, respectively.

1.8 Gene expressions

Messenger RNA (mRNA) expression of pro-angiogenic and stemness markers in DPSCs were evaluated by real-time reverse transcription polymerase chain reaction (PCR) with a TaqMan Gene Expression Cells-to-Ct Kit (Ambion, TX, USA).

Ten thousand DPSCs were seeded in a 60 mm culture dish and incubated in 4 mL of EM without or with surfen (0, 1, 5, or 10 μM). The same number of DPSCs cultured in 4 mL of GM without surfen was regarded as the control group. After 7 days, the cells were washed twice with cold PBS and collected by the cell scraper from the culture dish. Cell pellets were obtained by centrifugation at 1,000

rpm for 5 min and incubated with 50 μL of lysis solution at room temperature for 5 min. Then, 5 μL of stop solution was mixed into the lysate for 2 min to inactivate the lysis reagents.

Ten μL of cell lysates were reverse transcribed to synthesize complementary DNA (cDNA) by reacting with the pre-mixture of 25 μL of 2 x RT Buffer, 2.5 μL of 20 x RT Enzyme Mix, and 12.5 μL of Nuclease-Free Water, under the following conditions: 37°C for 60 min, then 95°C for 5 min. Subsequently, 4.0 μL of cDNA, 10 μL of TaqMan Gene Expression Master Mix, 5.0 μL of nuclease-free water, and 1.0 μL of each primer [*vascular endothelial growth factor A* (*VEGFA*), *C-X-C motif chemokine ligand 1* (*CXCL1*), *Nanog*, *glyceraldehyde 3-phosphate dehydrogenase* (*GAPDH*); Applied Biosystems] were mixed up to conduct the PCR by the StepOne Real-time PCR System (Applied Biosystems). The experiments were repeated four times. One of the replicates from control was utilized to normalize all samples. Expression levels of *VEGFA*, *CXCL1*, and *Nanog* were calculated relative to those of *GAPDH* using the $2^{-\Delta\Delta Ct}$ method. Each gene expression level among all groups was analyzed by the one-way ANOVA and Tukey's HSD test with a significance level of $P < 0.05$.

2. Results

2.1 HS production in the presence of surfen

HS production of DPSCs in the presence or absence of surfen is shown in Figure 1. At 7 days of culture, HS concentration in DPSCs cultured in GM or EM without surfen was 10.73 ± 1.03 and 11.86 ± 1.46 μg/mL, respectively, and no significant difference was observed. With increasing dosages of surfen, the yields of HS gradually decreased in both media. HS production in the DPSCs treated with 10 μM of surfen was reduced by approximately half when compared with those without surfen, demonstrating 5.86 ± 1.13 and 6.67 ± 0.71 μg/mL for GM and EM, respectively. These results indicated that surfen could act as an HS antagonist to reduce HS production in DPSCs.

2.2 DPSC proliferation under surfen treatment

Morphological alteration from a spindle to irregular shape was observed in DPSCs cultured with 10 μM surfen-containing EM, however no statistical differences in cell numbers were observed among the experimental conditions at day 1 (Figures 2 and 3). At 3 days of endothelial induction, a significant difference

in cell numbers was observed only between DPSCs alone and 10 μM surfen-treated DPSCs; thereafter, cell proliferation under EM culture was significantly suppressed by increasing the concentrations of surfen. Notably, no significant difference in cell proliferation was detected for cells cultured in GM at corresponding observation times (Figure 3).

2.3 Sprouting ability of DPSCs in presence of surfen

DPSCs possessed great sprouting ability in the EM without surfen, and reticular structures were gradually formed up to 14 days (Figure 4A). The sprouting ability of DPSCs was suppressed by the addition of surfen. Cells cultured in surfen (10 μM)-containing EM displayed a few clusters with short sprouts that were unconnected each other, even after 14 days of induction.

Image analyses revealed that the numbers and total lengths of sprouting branches were significantly decreased in DPSCs cultured with increasing dosages of surfen (Figure 4B, C).

2.4 Devitalization and revitalization of sprouting ability

The experimental design for sprouting devitalization was described in Figure 5A.

Reticular-like structures of DPSCs were formed during the first 7 days of endothelial induction (Figure 5B(I, II)). It was shown that DPSCs arrested the formation of capillary-like networks by surfen addition (Figure 5B(III–IV)). Statistically, DPSCs cultured with 10 μM of surfen formed significantly less and shorter branches than the cells cultured with 5 μM surfen (Figure 5C, D).

The experimental design for sprouting revitalization was described in Figure 6A. Although the formation of capillary sprouts was impaired upon exposure to surfen during the first 7 days, both the number and total length of branches significantly increased with the removal of surfen, indicating that sprouting ability of DPSCs was revitalized (Figure 6(B–D)).

2.5 Viability of DPSCs in presence of surfen

Live/dead staining revealed that sprouting areas developed by living cells gradually decreased with increasing surfen concentrations throughout the culture period. Although dead cells increased with surfen stimulation, there were fewer dead DPSCs compared with the areas occupied by living cells among all conditions (Figure 7).

2.6 Gene expressions of DPSCs upon exposure to surfen

Figure 8 demonstrates the endothelial differentiation and stemness properties of DPSCs in the presence of sufen, as determined by real-time PCR. Expression of pro-angiogenic markers *VEGFA* and *CXCL1* was significantly greater in DPSCs cultured in EM compared with GM at day 7, with fold changes of *VEGFA* and *CXCL1* expression in EM of 2.78 ± 0.71 and 7.17 ± 4.84, respectively. Significant declines of pro-angiogenic markers were observed in response to increasing dosages of surfen. The expression of stemness marker *Nanog* was reduced to 0.10 ± 0.02 when the cells were cultured with EM, and surfen addition resulted in an increase in *Nanog* expression.

3. Discussion

The biological function of HS is largely determined by HS chain interaction with protein ligands [54]. Multiple agents for antagonizing HS-protein interactions have been developed to inhibit tumor angiogenesis, including heparin mimetics [55,56], sugar analogs [57], small molecule competitors that bind with HS [58], and novel compounds that inhibit HS biosynthesis and sulfation [59]. In this research, surfen, a small antagonist of HS, was utilized to inhibit the HS-protein interaction.

Surfen molecule was first described as an excipient of depot insulin production, with the advantages of low toxicity and antibacterial properties [60]. It was demonstrated that surfen interferes with the binding of semen-derived enhancer of viral infection (SEVI) to both target cells and human immunodeficiency virus (HIV) type 1 virion, subsequently inhibiting SEVI-mediated HIV type 1 infection [61]. In addition, surfen has been shown to reduce inflammation and inhibit remyelination of multiple sclerosis by the murine model [62]. Surfen also blocks C5a receptor binding and acts as the inhibitor of anthrax lethal factor [63,64].

In 1961, it was first reported that surfen possesses the heparin-neutralizing property by using oral administration in mice and rabbit models [65]. Recently, it was demonstrated that positively charged surfen could bind to the negatively charged heparin/HS by electronic interactions [52]. Structurally, the aminoquinolin moieties of surfen and carboxylate or sulfate groups of heparin/HS glycosaminoglycan constitute the key binding interactions [58,66]. Surfen occupied the binding site between heparin/HS and growth factors, subsequently altering various cellular biological activities dependent on heparin/HS [58] (Figure 9). Tube formation of primary murine endothelial cells induced by bFGF or VEGF

was reportedly blocked in response to surfen [52]. Moreover, FGF signaling, which is responsible for regulating angiogenesis, was blocked by both surfen and its analogs through antagonism of HS-protein interactions in mouse embryonic fibroblasts [58]. Therefore, in this study, surfen was used to determine the DPSC vasculogenic property under endothelial induction.

It was previously reported that surfen suppressed bFGF binding in wild-type Chinese hamster ovary cells in a dose-dependent manner, with half maximal inhibitor concentration (IC_{50}) at 5 μM and with 95% inhibition at 10 μM. However, 20 μM of surfen resulted in reduced inhibitory function [52]. Consequently, 10 μM was selected as the highest concentration of surfen to explore its impact on DPSC proliferation and vasculogenesis.

The numbers of DPSCs with endothelial induction were greater than those cultured with GM. This finding could be explained by the supplementary growth factors (e.g., FGF, VEGF) included in EM, which offer adequate nutrients for cell proliferation. However, cell proliferation undergoing endothelial differentiation was remarkably suppressed by surfen addition. In contrast, no significant difference was observed in cells cultured in GM. This result might be attributed to the competitive binding of surfen to HS, which reduces the availability of binding

sites for pro-angiogenic factors (e.g., FGF and VEGF) included in EM. Thus, ECM interactions were impeded by surfen such that cells could not sufficiently exploit pro-angiogenic factors. However, few growth factors were included in GM, suggesting that cell proliferation in GM was unaffected even in the presence of 10 μM surfen.

Matrigel is composed of solubilized basement membrane matrix extracted from Engelbreth-Holm-Swarm mouse sarcoma cells, which could mimic the native ECM by replicating cell-ECM interaction [67]. Matrigel has been widely used in stem cell culture because it can create a 3D suitable cellular microenvironment for the maintenance of cell self-renewal and pluripotency [68,69]. Cells seeded on Matrigel are capable to grow, differentiate in response to the media, and migrate by secreting various matrix metalloproteinases under external stimulation. It was previously reported that DPSCs under endothelial induction displayed the sprouting capacity by migrating and inserting the branches into the Matrigel layer for up to 50 μm thickness [22]. Therefore, “number of branches” and “total branching length” were selected to describe the sprouting capacity of endothelial differentiated DPSCs in this study. It was observed that the formation of reticular-like structures by DPSCs was suppressed

by the addition of surfen without affecting cell viability. Noticeably, the deactivation of sprouting ability was recovered with the removal of surfen. These results demonstrated that the functional inhibition of HS by surfen addition hampered the capillary sprouting of DPSCs.

Genetically, it was revealed that expression of endothelial-related markers (e.g., *VEGFA* and *CXCL1*) was significantly upregulated in DPSCs cultured with EM than the cells with GM, indicating DPSCs possessed great endothelial differentiation potential. However, surfen addition resulted in the downregulation of pro-angiogenic marker expression and upregulation of stemness-related marker expression (e.g., *Nanog*). These results suggested that endothelial differentiation of DPSCs was impeded and stemness property of DPSCs was maintained by using surfen. More detailed signaling mechanisms by which the vasculogenic potential of DPSCs was suppressed by surfen remain to be investigated.

4. Summary

Surfen, an HS antagonist, suppressed the cell proliferation and sprouting capacity without affecting the cell viability of DPSCs undergoing endothelial

differentiation. Expression of pro-angiogenic markers significantly declined with increasing dosages of the HS antagonist; in contrast, the expression of stemness marker increased.

Chapter 2: Vasculogenic behaviors of *EXT1*-silenced DPSCs

Objectives

- To assess the HS production after *EXT1* silencing in DPSCs.
- To determine proliferative and vasculogenic behaviors of *EXT1*-silenced DPSCs *in vitro.*
- To evaluate gene expression patterns in *EXT1*-silenced DPSCs.

1. Materials and methods

1.1 Heparan sulfate

Aqueous stock solution of heparan sulfate (10 mg/mL) was prepared by dissolving 10 mg of heparan sulfate powder (MedChemExpress, NJ, USA) in 1 mL of ultrapure water. The stock solution was kept at -20°C and working solution was freshly prepared based on the stock concentration.

1.2 *EXT1* silencing

The expression of *EXT1* was silenced by using lentiviral short hairpin RNA (shRNA). DPSC suspension at 1 x 10^6 cells/mL was prepared with GM and then

mixed up with lentiviral particles (10^8 TU/mL, Sigma-Alidrich) to silence *EXT1* in DPSCs. Meanwhile, lentiviral particles with scramble sequence control with green fluorescent protein (GFP; Sigma-Aldrich) were transfected to establish the sh-control DPSCs. Both cells were incubated at 37°C for 30 min, and then seeded in the 60 mm culture dish. Following 2 days of culture, transduced cells were selected with 2 μg/mL of puromycin (Invitrogen) for 1 week.

EXT1-silenced and sh-control DPSCs at a density of 500 cells/cm^2 were seeded in a 60 mm culture dish and cultured with EM. Following incubation for 7 and 14 days, gene silencing efficiency was evaluated by real-time PCR using *EXT1* specific primer (Applied Biosystems), as described in 1.8 of Chapter 1. The experiments were repeated four times. One of the replicates from sh-control DPSCs was set as “1” and utilized to normalize all samples. The expression level of *EXT1* was calculated relative to those of the reference gene *GAPDH* using the $2^{-\Delta\Delta Ct}$ method. The data of *EXT1* expressions between two groups were analyzed by the Student’s *t*-test with a significance level of $P < 0.05$.

EXT1 silencing efficiency was also evaluated by western blotting assay. *EXT1*-silenced and sh-control DPSCs at a density of 500 cells/cm^2 were seeded in a 60 mm culture dish. After culturing with EM for 7 and 14 days, cell protein

lysates were obtained by treating with RIPA lysis buffer, as described in 1.3 of Chapter 1. The concentration of each protein sample was measured using Bio-Rad protein assay dye reagent concentrate (Bio-Rad). The mixture of 15 μg of each protein lysate, 4 μL of NuPAGE (Invitrogen), and 1.6 μL of dithiothreitol (DTT, 0.5 M) was boiled at 95°C for 5 min to allow protein denaturation, and then these specimens were kept at -80°C for further use.

The mixture containing an equal amount of protein (15 μg), NuPAGE, and DTT was loaded into the designated well created by a 1 mm 12-well comb (Novex, CA, USA), and separated using 9% SDS-PAGE gel at 130 V for 90 min to conduct electrophoresis. The loaded protein on the gel was transferred to a poly(vinylidene fluoride) membrane (Bio-Rad) at 200 mA for 2 h under cooling condition. After blocking with 5% non-fat milk (Morinaga, Tokyo, Japan) for 30 min, the membrane was incubated with mouse monoclonal primary antibody against human EXT1 (1:500; Santa Cruz Biotechnology) and mouse monoclonal primary antibody against human β-actin (1:4000; Proteintech, CA, USA) overnight at 4°C. The following day, membrane was incubated with the horseradish peroxidase-conjugated goat anti-mouse secondary antibody (1:5000; GE Healthcare, Buckinghamshire, UK) for 1 h at room temperature with gentle

shaking. Finally, immunoreactive proteins were visualized by Gene Gnome5 chemiluminescent imaging system (Syngene, Cambridge, UK) using the Chemi-Lumi One L kit (Nacalai Tesque).

1.3 HS production

EXT1-silenced and sh-control DPSCs at an initial density of 500 cells/cm^2 were cultured with EM for 7 and 14 days. Subsequently, both cells were lysed in RIPA buffer and HS production was quantified by ELISA, as mentioned in 1.3 of Chapter 1. The experiments were repeated four times. The data of HS production with *EXT1* silencing were analyzed by the Student's *t*-test with a significance level of $P < 0.05$.

1.4 Cell proliferation

The proliferative ability of transduced DPSCs was evaluated using a WST-8 assay kit (Dojindo). *EXT1*-silenced DPSCs were seeded in 96-well plates at a density of 500 cells/well and maintained in GM or EM. After 1, 3, or 5 days of culture, 10 µL of WST-8 solution was added to each well, and plates were incubated for an additional 2 h. The absorbance of each well at 450 nm was

measured using a microplate reader (Bio-Rad). The experiments were repeated four times. Relative cell numbers among groups were analyzed by the one-way ANOVA and Tukey's HSD test with a significance level of $P < 0.05$. In addition, transduced cells were observed by the light microscope (CK40-F100) at corresponding time points.

1.5 Vascular sprouting

EXT1-silenced DPSCs were seeded on the Matrigel-precoated 24-well plates at the density of 1×10^4 cells/well and maintained in EM with or without 168 μM (100 μg/mL) of HS. The sh-control DPSCs at the same density were also cultured on the Matrigel-precoated plates by using EM. Reticular-like structure formed by the cells was observed using the light microscopy (CK40-F100) at 1, 3, 7, and 14 days of culture. Four independent images from different views of each group were randomly selected and the number and total length of branches were counted by ImageJ. The obtained data were statistically analyzed by utilizing the one-way ANOVA and Tukey's HSD test with a significance level of $P < 0.05$.

1.6 Gene expressions

The gene expression profile of *EXT1*-silenced DPSCs was examined by RNA sequencing according to the manufacturer's instructions. *EXT1*-silenced and sh-control DPSCs at the density of 500 cells/cm^2 were seeded in a 60 mm culture dish. After 14 days of endothelial induction, cells were rinsed twice with PBS to remove the dead cells and debris. Then, the cells were treated with 1 mL of TRIzol reagent (Thermo Fisher Scientific) for 5 min, and cell lysates were transferred to a 1.5 mL Eppendorf tube. The lysate was mixed with 200 μL of chloroform (Sigma-Aldrich), and centrifuged at 12,000 rpm for 15 min at 4°C. The supernatant was transferred to a 1.5 mL RNase-free tube (Thermo Fisher Scientific) and mixed with an equal volume of 70% ethanol (Kanto Chemical, Tokyo, Japan). Total RNA was extracted with an RNeasy Mini Kit (Qiagen, CA, USA), according to the manufacturer's instruction. RNA sequencing was performed using a sequencing system (Novaseq 6000; Illumina, CA, USA). The biological significance of differentially expressed genes (DEGs) was explored by volcano plot and gene ontology (GO) enrichment analysis using DESeq2.

Expression of pro-angiogenic and stemness markers in DPSCs was further evaluated by real-time PCR. Transfected cells were seeded in 60 mm culture dish at the same density as the cells for the RNA sequencing experiment.

Following endothelial induction for 7 or 14 days, these cells were evaluated on mRNA expression levels of *VEGFA*, *CXCL1*, *Nanog*, and *GAPDH* using a TaqMan Gene Expression Cells-to-Ct Kit (Ambion). Expression levels of *VEGFA*, *CXCL1*, and *Nanog* were calculated relative to those of *GAPDH* using the $2^{-\Delta\Delta Ct}$ method. One of the replicates from sh-control DPSCs was utilized to normalize all samples. The experiments were repeated four times. The statistical data of each expression between two groups were analyzed by the Student's *t*-test with a significance level of $P < 0.05$.

2. Results

2.1 *EXT1* silencing and HS production of DPSCs

The mRNA expression of *EXT1* was significantly decreased in *EXT1*-silenced DPSCs, with fold changes of 0.31 ± 0.05 and 0.45 ± 0.07 at 7 and 14 days of endothelial induction, respectively (Figure 10A). Western blotting assay demonstrated that EXT1 protein expressions decreased in *EXT1*-silenced DPSCs compared with the sh-control cells (Figure 10B). These results indicated that *EXT1* was successfully downregulated in both mRNA and protein levels by lentivirus shRNA. Additionally, it was found that *EXT1* silencing in DPSCs led to

lower production of HS compared with sh-control cells for up to 14 days of induction (Figure 11).

2.2 Proliferative ability of *EXT1*-silenced DPSCs

The morphology and proliferation of *EXT1*-silenced and sh-control DPSCs are shown in Figure 12. There was no difference in cell morphology among all groups for up to 3 days. The sh-control DPSCs in EM altered their polygonal morphology into small round shape at day 5 (Figure 12A). There was no significant difference in the cell numbers at 1 day between two types of cells; thereafter, the numbers of *EXT1*-silenced DPSCs were significantly lower when compared with sh-control transduced cells cultured in EM. The numbers of both cells cultured with EM were significanly greater than those cultured with GM at 5 days (Figure 12B).

2.3 Vasculogenic behavior of *EXT1*-silenced DPSCs *in vitro*

There is no difference in the cell sprouting among *EXT1*-silenced DPSCs with or without exogenous HS, as well as sh-control DPSCs at 1 and 3 days (Figure 13A). After 7 and 14 days of culture, *EXT1*-silenced DPSCs formed fewer capillary-like structures compared with sh-control DPSCs. The addition of exogenous HS

ameliorated the sprouting capacity of *EXT1*-silenced DPSCs. Quantitative analyses demonstrated that no significant difference in the number and total length of branches was found after 1 and 3 days of induction (Figure 13B, C). Thereafter, *EXT1*-silenced DPSCs developed fewer and shorter branches than those of sh-control cells; however, HS supplementation resulted in significant recovery of both numbers and total lengths of branches in *EXT1*-silenced DPSCs to levels comparable with sh-control cells.

2.4 Gene expression in *EXT1*-silenced DPSCs

Heatmap data based on hierarchical clustering displayed the difference in gene expression patterns between *EXT1*-silenced DPSCs and sh-control DPSCs (Figure 14). Furthermore, volcano plot analysis summarized significantly upregulated and downregulated genes (p adjust < 0.05, |fold change| > 2) in *EXT1*-silenced DPSCs (Figure 15). In particular, several downregulated genes involved in angiogenic processes (*e.g.*, *VCAM1*, *APOE*, and *LEP*) and HS sulfation modification (*e.g.*, *SULF1*) were detected and highlighted in Figure 15. A detailed list of downregulated genes related to angiogenesis and HS biosynthesis is shown in Table 1. The result of GO analysis shown in Figure 16

revealed that gene expressions associated with ECM organization and cell adhesion decreased in *EXT1*-silenced DPSCs. In addition, several biological processes, including angiogenesis and response to hypoxia, were significantly downregulated, suggesting a potential role of HS in regulating vascular formation of DPSCs. Conversely, silencing of *EXT1* resulted in the upregulation of several genes responsible for degradation of ECM (*e.g.*, *MMP1*, *MMP3*, and *PFN1*), and cell activities involved in the proteasome-mediated catabolic process and mitochondrial translational termination were significantly activated in *EXT1*-silenced DPSCs (Figures 15 and 16).

When expression of genes specifically related to endothelial differentiation and stemness properties were evaluated by real-time PCR (Figure 17), fold changes of *VEGFA* and *CXCL1* expression at day 7 in *EXT1*-silenced DPSCs were 0.66 ± 0.06 and 0.31 ± 0.08, respectively. Further, significant differences were detected after 14 days of induction (0.39 ± 0.07 and 0.07 ± 0.04) in these angiogenic gene expressions. Conversely, the fold change of *Nanog* expression in *EXT1*-silenced cells was significantly greater than that of sh-control cells throughout the culture period, demonstrating 1.44 ± 0.16 and 1.43 ± 0.19 at 7 and 14 days, respectively.

3. Discussion

Heparan sulfate biosynthesis is conducted through a complicated process composed of chain polymerization and modification [70]. Chain polymerization involves the formation of an initial polysaccharide backbone structure, consisting of repeating glucuronic acid and N-acetylglucosamine disaccharide units. As the chain is growing up, a series of chain modifications include the N-sulfation of glucosamine units and the epimerization of glucuronic acid to iduronic acid, followed by various sulfation extents at different positions with 2-O-, 6-O-, and 3-O-sulfotransferase [42,71,72].

EXT1/EXT2 heterooligomeric complex is known to be a rate-limiting glycosyltransferase during HS polymerization, which is responsible for initiating the addition of disaccharide units to the linkage region of HS [73–75]. Without EXT1 and EXT2 enzymes, the subsequent modifications are unable to progress, leading to alteration in the final HS structure. Specifically, it was demonstrated that EXT1 encodes the disaccharide units for the elongation of HS backbone structure, whereas EXT2 might only have the N-acetylglucosamine transferase activity [76–78].

Early studies demonstrated that mutation of *EXT1* may result in hereditary multiple exostoses in human, an autosomal dominant inherited genetic disorder characterized by multiple osteochondromas and limb bone deformity [73]. Notably, recent research reported that the endothelial cell-specific *EXT1*-knockout mice exhibited reduced HS expression in the brain vascular endothelium and suppressed glioblastoma growth, unveiling a possible role of EXT1 in modulating HS expression of vascular endothelial cells [79]. In this study, *EXT1*-silenced DPSCs were established to further confirm the impact of HS on endothelial differentiation and vasculogenic processes. Here, despite the fact that the lack of EXT1 resulted in a significant decrease in HS quantitation of DPSCs *in vitro*, *EXT1*-silenced DPSCs could still produce a certain amount of HS compared with sh-control cells. It was reported that both the mouse fibroblast mutant cell and human promyelocytic leukemia cell lines defective in *EXT1* expression could still produce small and short HS chains [80], which was consistent with the findings obtained in this study. *EXT1* silencing was expected to prevent the EXT1 and EXT1/EXT2 complex formation, although EXT2 alone might still produce a few amounts of unfunctional fragments of HS. Further investigations are required to determine the specific components and structures

of HS formed by *EXT1*-silenced DPSCs.

The numbers of *EXT1*-silenced and sh-control DPSCs with endothelial induction were greater than those cultured with GM. This result might be explained by the supplementary growth factors (e.g., FGF, VEGF) included in EM, which provide sufficient nutrients for cell survival and proliferation. In addition, the cell numbers of *EXT1*-silenced DPSCs were significantly smaller than sh-control cells both in GM and EM, suggesting that EXT1 deficiency led to lower proliferative capacity of DPSCs. Furthermore, *EXT1*-silenced DPSCs formed less capillary-like structures compared with sh-control transduced DPSCs, which could be rescued by the addition of 168 μM (100 μg/mL) of exogenous HS. This concentration was substantially greater than the endogenous HS produced by both the sh-control and *EXT1*-silenced DPSCs (20.43 ± 4.46 and 15.5 ± 1.46 μg/mL, respectively), since only the greater concentration could more effectively ameliorate the sprouting ability of *EXT1*-silenced DPSCs. Exogenous 100 μg/mL HS was previously reported to enhance the chondrogenesis and cartilage nodule formation of bone marrow-derived stem cells (BMSCs) *in vitro*, which also belong to MSCs and share a similar multipotent characteristic with DPSCs [81,82]. The underlying mechanism behind the regulation of external HS on the DPSC

sprouting ability was required, which might reveal other processes distinct from endogenous HS function. These findings demonstrated that EXT1 acts as a key regulator of sprouting and capillary network formation by DPSCs.

Genetically, reduced pro-angiogenic gene expression and increased expression of stemness markers were detected in *EXT1*-silenced cells compared with sh-control DPSCs. This result indicated that a lack of HS inhibited endothelial differentiation potential and, at least in part, maintained the stemness property of DPSCs. The fold change of *Nanog* expression of *EXT1*-silenced DPSCs was 1.44 ± 0.16 and 1.43 ± 0.19 at 7 and 14 days of endothelial induction compared with sh-control cells, whereas 10 μM surfen stimulation led to a substantial increase of *Nanog* expression when compared with DPSCs maintained in GM, with the fold change of 56.42 ± 10.50. This discrepancy might be attributed to the fact that DPSCs could differentiate into odontoblast or fibroblast lineages even in GM, which reduced its stemness property to some extent [83]. Furthermore, a high concentration (10 μM) of surfen could effectively bind with HS chains and occupy the binding sites between HS and growth factors, subsequently leading to the maintenance of cell stemness.

Matrix metalloproteinases (MMPs) are involved in the breakdown of ECM

during physiological and pathological processes including tissue repair and remodeling [84]. In this study, it was revealed that HS disruption resulted in the upregulation of *MMP1* and *MMP3*. A previous study reported that sulfated HS glycosaminoglycans could provide anchoring sites for the MMPs, and HS breakdown led to the release of MMPs into the external microenvironment [85]. However, Agere *et al*. [86] demonstrated that HS degradation by digestive enzymes caused a reduction in MMP1 and MMP13 expressions in human rheumatoid arthritis synovial fibroblast cells. The controversial results might be attributed to the upregulation of *MMPs* in current study was achieved by silencing *EXT1*, rather than enzymatic digestion of HS. These findings call for more in-depth investigation of the relationship between HS and MMP, which may reveal other underlying mechanisms independent of binding efficiency.

EXT1 knockdown was previously reported to induce chemosensitivity in melanoma cells by activating c-Jun N-terminal kinase (JNK) and MEK/ERK signaling [87]. In addition, EXT1 was proved to affect the chondrogenic differentiation of ATDC5 cells via the canonical Wnt/β-catenin signaling [88]. The underlying signaling transduction by which EXT1 regulates the vasculogenic behavior of DPSCs requires further exploration.

4. Summary

Silencing of *EXT1* expression in DPSCs by using a short hairpin RNA significantly altered their gene expression profile. In addition, *EXT1*-silenced DPSCs expressed lower levels of endothelial differentiation markers and displayed a reduced vascular formation capacity compared with sh-control DPSCs transduced with scrambled sequences. The sprouting ability of *EXT1*-silenced DPSCs was rescued by the supplementation of exogenous HS. All these results demonstrated that a lack of HS by silencing *EXT1* suppressed vasculogenic properties of DPSCs.

Chapter 3: Impact of HS on vascular formation *in vivo*

Objectives

- To investigate vasculogenesis of DPSCs using the mouse subcutaneous implantation model.
- To evaluate the vascular formation ability of *EXT1*-silenced DPSCs *in vivo*.

1. Materials and methods

The protocol of animal experiments is illustrated in Figure 18.

1.1 Cell-loaded scaffold

Cell-loaded scaffolds were prepared by modification of the method previously described [89–91]. Poly-L-lactic acid (PLLA) particles (Polysciences, Warrington, PA) were dissolved by 5% solution in chloroform (Wako). Then, sodium chloride (Wako) ranging from 250 to 425 μm in diameter was mixed with PLLA solution and cast within a polytetrafluoroethylene (PTFE) tube (PTC68; AS-ONE, Osaka, Japan) with an 8 mm internal diameter and 1 mm thickness. After 24 h, sodium chloride was leached away by using distilled water. The PLLA scaffold prepared was dried and then kept in a 50 mL centrifuge tube for further use.

The day before surgery, PLLA scaffold was sterilized and hydrophilized with a sequence of 99.5%, 90%, and 70% ethanol followed by washing three times with sterilized PBS. On a surgery day, 1×10^6 *EXT1*-silenced or sh-control DPSCs were resuspended in the 40 μL mixture at the ratio of 1:1 of Matrigel and GM. The cell-containing mixture was then seeded into the sterilized porous PLLA scaffold, incubating at 37°C for 30 min to allow cell attachment and Matrigel polymerization.

1.2 Subcutaneous implantation model

All animal experiments followed ARRIVE (Animal Research: Reporting of *In Vivo* Experiments) guidelines and a strict protocol was approved by the Animal Experiments Committee of Osaka University Graduate School of Dentistry (Approval No. 26-021-0). Five 6-week-old male immunodeficient mice (CB.17. SCID; CLEA Japan, Tokyo, Japan) weighing 18 - 22 g were used in the experiments. Animals were kept in a specific pathogen-free environment with barriers and a controlled light cycle, providing sterile food and water ad libitum.

For the surgical procedure, SCID mice were anesthetized intraperitoneally by a mixture of 0.3 mg/kg of medetomidine (Domitor; Nippon Zenyaku Kogyo,

Tokyo, Japan), 4.0 mg/kg of midazolam (Dormicum; Maruishi Pharmaceutical, Osaka, Japan), and 5.0 mg/kg of butorphanol (Vetorphale; Meiji Seika Kaisha, Tokyo, Japan)). After anesthesia, the dorsal hair was shaved off, and a 15 mm of subcutaneous incision was created with a disposable scalpel (No. 15; Feather Safety Razor, Osaka, Japan). Subsequently, *EXT1*-silenced or sh-control DPSCs-loaded scaffolds were transplanted into the subcutaneous space bilaterally of mice, and incisional wound was closed with an absorbable suture (Nescosuture 4-0; Alfresa Pharma, Osaka, Japan).

1.3 Histological observation

After 5 weeks, specimens were harvested and then fixed with 10% buffered formalin phosphate (Wako) for 48 h. The PLLA scaffold was retrieved from the PTFE tube and embedded in paraffin by using the Cell & Tissue Processor CT-Pro20 (Genostaff, Tokyo, Japan) for 24 h. Paraffin sections of 5 μm thickness were prepared by using a microtome (2125RT; Leica, Wetzlar, Germany) and placed on glass slides (Matsunami, Osaka, Japan).

1.3.1 Toluidine blue and HE staining

The sulfated glycosaminoglycans in tissue section were visualized by toluidine blue staining. Toluidine blue is a basic thiazine metachromatic dye that has a high affinity for acidic tissue components, such as sulfate groups. The sections were deparaffinized by lemosol (Wako), rehydrated using a sequence of phased dilutions of ethanol. The rehydrated sections were then stained with 0.05% toluidine blue solution (Wako) for 5 min. After rinsing with the distilled water for 5 min, stained sections were hydrated and covered with the MGK-S mounting solution (Matsunami). Images were captured with a CCD camera (DS-Fi2; Nikon, Tokyo, Japan) attached to a light microscope (ECLIPSE Ci-L; Nikon).

For hematoxylin and eosin (HE) staining, rehydrated sections were stained with hematoxylin (Wako) for 5 min, rinsed with flowing water for 5 min, and then stained with 0.5% eosin Y (Wako) for 5 min. Stained sections were observed with a light microscope (ECLIPSE Ci-L) equipped with a CCD camera. Five independent views were randomly selected for each group, and the number of blood-containing vessels per unit area was measured. The results for *EXT1*-silenced and sh-control cell-seeded specimens were analyzed by the Student's *t*-test with a significance level of $P < 0.05$.

1.3.2 Immunofluorescence staining

Immunofluorescence staining was conducted to observe the DPSC-derived vasculature. Rehydrated sections underwent epitope retrieval with 1 mg/mL of trypsin from porcine pancreas (Sigma-Aldrich) for 1 h in a 37°C incubator. After blocking with PBS containing 0.3% Triton X-100 (Alfa Aesar, Lancashire, UK) and 0.1% w/v bovine serum albumin (Sigma-Aldrich) for 30 min, sections were incubated with mouse monoclonal primary antibodies against human HS (10E4 epitope; 1:100; US Biological Life Sciences, CA, USA), CD31 (1:50; Dako, CA, USA), von Willebrand factor (vWF, 1:200; Proteintech), and a rabbit polyclonal antibody against GFP (1:200; Invitrogen) for overnight at 4°C. Immunoreactive proteins were visualized by using Alexa Fluor 488 goat anti-mouse IgG (1:250; Invitrogen), Alexa Fluor 568 goat anti-mouse IgG (1:200; Invitrogen), and Alexa Fluor 594 goat anti-rabbit IgG (1:250; Invitrogen) for 1 h without the light at room temperature. All antibodies utilized in this experiment were diluted by the Antibody Diluent (Agilent, CA, USA). Nuclear staining was performed by Hoechst 33342 (1:1000; Invitrogen) for 5 min. After sealing with the VECTASHIELD Mounting Medium (Funakoshi, Tokyo, Japan), the stained sections were observed with a fluorescence microscope (TE2000) coupled with a CCD camera.

2. Results

2.1 Toluidine blue and HE staining

Stained intensity by the toluidine blue was lower in the specimens loaded with *EXT1*-silenced DPSCs than that with sh-control cells (Figure 19A), indicating that the polysaccharide produced by *EXT1*-silenced DPSCs was less than sh-control DPSCs. The numbers of blood-containing vessels for the scaffolds seeded with *EXT1*-silenced DPSCs was 14.6 ± 5.68 per unit area, and significantly smaller compared with specimens loaded with sh-control DPSCs which showed 26.4 ± 8.20 per unit area (Figure 19B, C).

2.2 Immunofluorescence staining

Immunofluorescence staining demonstrated that HS was distributed around the human-specific CD31-positive blood vessels in the DPSCs-loaded scaffold (Figure 20). In addition, GFP-transduced DPSCs formed blood cell-containing vessels and these vessels were positive for human-specific CD31 and vWF (Figure 21).

3. Discussion

The tooth slice/scaffold of dental pulp tissue engineering model has been developed as a research method for investigating neovascularization and dentinogenesis of dental stem cells [89,92,93]. It was reported that the pulp viability and vasculature were successfully maintained after transplanting the human tooth slice in the immunodeficient mice subcutaneously for 7 days [92]. Additionally, blood cell-containing vascular structures were observed within the stem cells from human exfoliated deciduous teeth (SHED) loaded-tooth slice after 14 days of implantation, indicating that the blood vessels within the specimen were anastomosed with the host vasculature [94]. Furthermore, reparative dentin-like tissues were deposited around the dentin layer when the human DPSC/dentin complex was transplanted into the immunodeficient mice [95]. All these previous data demonstrated that functional dental pulp-like tissue was formed in the tooth slice/scaffold model. In this study, the tooth slice/scaffold model was modified and the undegradable PTFE tube was utilized as the container of the cell-loaded scaffold, because the current study aimed to elucidate the DPSC vasculogenic process regulated by HS *in vivo*. Furthermore, the conventional tooth slice was obtained from the cervical area of healthy wisdom

teeth, reaching the volume of 29 - 43 mm^3 of slice model with 1 mm thickness [89, 93]. As a result, the internal diameter of 8 mm with 1-mm-thick ring was selected, which could create a similar space as a tooth slice. Considering the biocompatibility and undegradability, it was believed that PTFE rings could be an alternative to tooth slice to investigate the vascularization of the DPSC-loaded specimens [96,97].

In the mice model, *EXT1*-silenced DPSCs formed less polysaccharide and fewer functional microvessels exhibiting host blood cells inside, when compared with those of sh-control DPSCs. Colocalization of human-specific HS and CD31 expression was detected in the sample loaded with GFP-transduced DPSCs. This result implicated that DPSC vasculature formation was regulated by HS *in vivo.* Although it was difficult to determine the precise ratio of blood vessels formed by human-derived GFP-transduced DPSCs, colocalization of blood-containing vascular-like structures positive for the human-specific pro-angiogenic proteins (e.g., CD31 and vWF) and GFP expression in microvessels could be observed in specimens seeded with sh-control DPSCs. These results demonstrated that vascular endothelial cells originating from DPSCs formed nascent blood vessels and anastomosed with the host vasculature. Taken

together, these data demonstrate that EXT1 plays an important role in vascular formation originating from DPSCs, and HS is essential for modulating vasculogenic processes of DPSCs *in vivo*.

4. Summary

EXT1-silenced DPSCs produced fewer amounts of polysaccharides and formed fewer functional vessels than sh-control DPSCs in the SCID mice model. HS localization and CD31 expression were observed in the specimen loaded with GFP-transduced DPSCs, and lumen-like structures positive for human CD31 and vWF were formed by GFP–transduced DPSCs. All the data demonstrated that HS supported the development of functional microvessels derived from DPSCs *in vivo*.

General conclusion

DPSCs were recently reported to be capable of differentiating into vascular endothelial lineages. During this process, DPSC responses to the extracellular microenvironment and cell-ECM interaction are critical in regulating their ultimate cell fate. In this study, HS glycosaminoglycan, an integral component of ECM and key regulator of various biological activities, was focused, to explore its significance to endothelial differentiation and vasculogenesis of DPSCs.

The vasculogenic property of DPSCs was inhibited by using an HS inhibitor (surfen) and by genetic silence of *EXT1* responsible for HS biosynthesis. The mice model further confirmed that HS is essential for functional microvessel formation originating from DPSCs *in vivo*. Future investigations are necessary to ascertain whether EXT1/HS regulates the vasculogenesis of other MSC types, such as bone marrow- and adipose-derived cells. Moreover, further investigation is required to determine the mechanisms by which HS glycosaminoglycan mediates the vasculogenic behavior of DPSCs. Nevertheless, considering the complex structure and various sulfation extent of HS, future studies are warranted to explore the specific component and sequence of HS chains that can control the vasculogenic process.

Collectively, the present study demonstrates that HS is required for the regulation of endothelial differentiation and vasculogenesis of DPSCs, thus opening new perspectives for applications of HS glycosaminoglycan to tissue engineering and dental pulp regeneration.

References

[1] Rademakers T, Horvath JM, Van Blitterswijk CA, LaPointe VL. Oxygen and nutrient delivery in tissue engineering: Approaches to graft vascularization. J Tissue Eng Regener Med. 2019;13(10):1815–1829.

[2] Fu J, Wang DA. *In situ* organ-specific vascularization in tissue engineering. Trends Biotechnol. 2018;36(8):834–849.

[3] Burton AC. Relation of structure to function of the tissues of the wall of blood vessels. Physiol Rev. 1954;34(4):619–642.

[4] Gottweis H, Gaskell G, Starkbaum J. Connecting the public with biobank research: Reciprocity matters. Nat Rev Genet. 2011;12(11):738–739.

[5] Hoeben ANN, Landuyt B, Highley MS, Wildiers H, Van Oosterom AT, De Bruijn EA. Vascular endothelial growth factor and angiogenesis. Pharmacol Rev. 2004;56(4):549–580.

[6] Jain RK, Au P, Tam J, Duda DG, Fukumura D. Engineering vascularized tissue. Nat Biotechnol. 2005;23(7):821–823.

[7] Nomi M, Atala A, De Coppi P, Soker S. Principals of neovascularization for tissue engineering. Mol Aspects Med. 2002;23(6):463–483.

[8] Grunewald M, Avraham I, Dor Y, Bachar-Lustig E, Itin A, Jung S, Chimenti S, Landsman L, Abramovitch R, Keshet E. VEGF-induced adult neovascularization: Recruitment, retention, and role of accessory cells. Cell. 2006;124(1):175–189.

[9] Smadja DM. Vasculogenic stem and progenitor cells in human: Future cell therapy product or liquid biopsy for vascular disease. Stem Cells: Adv Exp Med Biol. 2019;1201:215–237.

[10] Isner JM, Asahara T. Angiogenesis and vasculogenesis as therapeutic strategies for postnatal neovascularization. J Clin Invest. 1999;103(9):1231–1236.

[11] Gronthos S, Brahim J, Li W, Fisher LW, Cherman N, Boyde A, DenBesten P, Robey PG, Shi S. Stem cell properties of human dental pulp stem cells. J Dent Res. 2002;81(8):531–535.

[12] Gronthos S, Mankani M, Brahim J, Robey PG, Shi S. Postnatal human dental pulp stem cells (DPSCs) *in vitro* and *in vivo*. Proc Natl Acad Sci USA. 2000;97(25):13625–13630.

[13] Luke AM, Patnaik R, Kuriadom S, Abu-Fanas S, Mathew S, Shetty KP. Human dental pulp stem cells differentiation to neural cells, osteocytes and adipocytes-An *in vitro* study. Heliyon. 2020;6(1):e03054.

[14] Bergamo MT, Zhang Z, Oliveira TM, Nör JE. VEGFR1 primes a unique cohort of dental pulp stem cells for vasculogenic differentiation. Eur Cells Mater. 2021;41:332-344.

[15] Janebodin K, Zeng Y, Buranaphatthana W, Ieronimakis N, Reyes M. VEGFR2-dependent angiogenic capacity of pericyte-like dental pulp stem cells. J Dent Res. 2013;92(6):524–531.

[16] Katata C, Sasaki JI, Li A, Abe GL, Nör JE, Hayashi M, Imazato S. Fabrication of vascularized DPSC constructs for efficient pulp regeneration. J Dent Res. 2021;100(12):1351–1358.

[17] Chen Y, Huang H, Li G, Yu J, Fang F, Qiu W. Dental-derived mesenchymal stem cell sheets: A prospective tissue engineering for regenerative medicine. Stem Cell Res Ther. 2022;13(1):38.

[18] Granz CL, Gorji A. Dental stem cells: The role of biomaterials and scaffolds in developing novel therapeutic strategies. World J Stem Cells. 2020;12(9):897–921.

[19] Li X, Ma C, Xie X, Sun H, Liu X. Pulp regeneration in a full-length human tooth root using a hierarchical nanofibrous microsphere system. Acta Biomater. 2016;35:57–67.

[20] Zhang Z, Nör F, Oh M, Cucco C, Shi S, Nör JE. Wnt/β-catenin signaling determines the vasculogenic fate of postnatal mesenchymal stem cells. Stem Cells. 2016;34(6):1576–1587.

[21] Zhang Z, Oh M, Sasaki JI, Nör JE. Inverse and reciprocal regulation of p53/p21 and Bmi-1 modulates vasculogenic differentiation of dental pulp stem cells. Cell Death Dis. 2021;12(7):644.

[22] Sasaki JI, Zhang Z, Oh M, Pobocik AM, Imazato S, Shi S, Nör JE. VE-

cadherin and anastomosis of blood vessels formed by dental stem cells. J Dent Res. 2020;99(4):437-445.

[23] Theocharis AD, Skandalis SS, Gialeli C, Karamanos NK. Extracellular matrix structure. Adv Drug Delivery Rev. 2016;97:4–27.

[24] Kular JK, Basu S, Sharma RI. The extracellular matrix: Structure, composition, age-related differences, tools for analysis and applications for tissue engineering. J Tissue Eng. 2014;5:2041731414557112.

[25] Xing H, Lee H, Luo L, Kyriakides TR. Extracellular matrix-derived biomaterials in engineering cell function. Biotechnol Adv. 2020;42:107421.

[26] Zhang W, Liu Y, Zhang H. Extracellular matrix: an important regulator of cell functions and skeletal muscle development. Cell Biosci. 2021;11(1):65.

[27] Huang G, Greenspan DS. ECM roles in the function of metabolic tissues. Trends Endocrinol Metab. 2012;23(1):16-22.

[28] Assis-Ribas T, Forni MF, Winnischofer SMB, Sogayar MC, Trombetta-Lima M. Extracellular matrix dynamics during mesenchymal stem cells differentiation. Dev Biol. 2018;437(2):63-74.

[29] Smith LR, Cho S, Discher DE. Stem cell differentiation is regulated by extracellular matrix mechanics. Physiol. 2018;33(1):16-25.

[30] Marchand M, Monnot C, Muller L, Germain S. Extracellular matrix scaffolding in angiogenesis and capillary homeostasis. Semin Cell Dev Biol. 2019;89:147–156.

[31] Sottile J. Regulation of angiogenesis by extracellular matrix. Biochim Biophys Acta Rev Cancer. 2004;1654(1):13-22.

[32] Frangogiannis NG. The Extracellular matrix in ischemic and nonischemic heart failure. Circ Res. 2019;125(1):117-146.

[33] Ravi S, Caves JM, Martinez AW, Xiao J, Wen J, Haller CA, Davis ME, Chaikof EL. Effect of bone marrow-derived extracellular matrix on cardiac function after ischemic injury. Biomater. 2012;33(31):7736–7745.

[34] Li H, Bao M, Nie Y. Extracellular matrix–based biomaterials for cardiac regeneration and repair. Heart Fail Rev. 2021;26(5):1231–1248.

[35] Kristofik NJ, Qin L, Calabro NE, Dimitrievska S, Li G, Tellides G, Niklason LE, Kyriakides TR. Improving *in vivo* outcomes of decellularized vascular grafts via incorporation of a novel extracellular matrix. Biomater. 2017;141:63–73.

[36] Ciuffreda MC, Malpasso G, Chokoza C, Bezuidenhout D, Goetsch KP, Mura M, Pisano F, Davies NH, Gnecchi M. Synthetic extracellular matrix mimic hydrogel improves efficacy of mesenchymal stromal cell therapy for ischemic cardiomyopathy. Acta Biomater. 2018;70:71–83.

[37] Ungerleider JL, Johnson TD, Hernandez MJ, Elhag DI, Braden RL, Dzieciatkowska M, Osborn KG, Hansen KC, Mahmud E, Christman KL. Extracellular matrix hydrogel promotes tissue remodeling, arteriogenesis, and perfusion in a rat hindlimb ischemia model. JACC Basic Transl Sci. 2016;1(1-2):32-44.

[38] Hassell JR, Kimura JH, Hascall VC. Proteoglycan core protein families. Annu Rev Biochem. 1986;55:539–567.

[39] Iozzo RV, Schaefer L. Proteoglycan form and function: A comprehensive nomenclature of proteoglycans. Matrix Biol. 2015;42:11–55.

[40] Rudd TR, Skidmore MA, Guerrini M, Hricovini M, Powell AK, Siligardi G, Yates EA. The conformation and structure of GAGs: Recent progress and perspectives. Curr Opin Struct Biol. 2010;20(5):567–574.

[41] Laremore TN, Zhang F, Dordick JS, Liu J, Linhardt RJ. Recent progress and applications in glycosaminoglycan and heparin research. Curr Opin Chem Biol. 2009;13(5-6):633–640.

[42] Li JP, Kusche-Gullberg M. Heparan sulfate: biosynthesis, structure, and function. Int Rev Cell Mol Biol. 2016;325:215–273.

[43] Gómez Toledo A, Sorrentino JT, Sandoval DR, Malmström J, Lewis NE, Esko JD. A systems view of the heparan sulfate interactome. J Histochem Cytochem. 2021;69(2):105–119.

[44] Pellegrini L. Role of heparan sulfate in fibroblast growth factor signalling: A structural view. Curr Opin Struct Biol. 2001;11(5):629–634.

[45] Forsten-Williams K, Chu CL, Fannon M, Buczek-Thomas JA, Nugent MA.

Control of growth factor networks by heparan sulfate proteoglycans. Ann Biomed Eng. 2008;36(12):2134–2148.

[46] Xu D, Fuster MM, Lawrence R, Esko JD. Heparan sulfate regulates VEGF165- and VEGF121-mediated vascular hyperpermeability. J Biol Chem. 2011;286(1):737–745.

[47] van Wijk XM, van Kuppevelt TH. Heparan sulfate in angiogenesis: A target for therapy. Angiogenesis. 2014;17(3):443–462.

[48] Shi J, Fan C, Zhuang Y, Sun J, Hou X, Chen B, Xiao Z, Chen Y, Zhan Z, Zhao Y, Dai J. Heparan sulfate proteoglycan promotes fibroblast growth factor-2 function for ischemic heart repair. Biomater Sci. 2019;7(12):5438–5450.

[49] Chan SJ, Esposito E, Hayakawa K, Mandaville E, Smith RAA, Guo S, Niu W, Wong PT, Cool SM, Lo EH, Nurcombe V. Vascular endothelial growth factor 165-binding heparan sulfate promotes functional recovery from cerebral ischemia. Stroke. 2020;51(9):2844–2853.

[50] Gupta P, Oegema Jr TR, Brazil JJ, Dudek AZ, Slungaard A, Verfaillie CM. Structurally specific heparan sulfates support primitive human hematopoiesis by formation of a multimolecular stem cell niche. Blood. 1998;92(12):4641–4651.

[51] Harfouche R, Hentschel DM, Piecewicz S, Basu S, Print C, Eavarone D, Kiziltepe T, Sasisekharan R, Sengupta S. Glycome and transcriptome regulation of vasculogenesis. Circulation. 2009;120(19):1883–1892.

[52] Schuksz M, Fuster MM, Brown JR, Crawford BE, Ditto DP, Lawrence R, Glass CA, Wang L, Tor Y, Esko JD. Surfen, a small molecule antagonist of heparan sulfate. Proc Natl Acad Sci USA. 2008;105(35):13075–13080.

[53] Reijmers RM, Groen RW, Rozemuller H, Kuil A, de Haan-Kramer A, Csikós T, Martens AC, Spaargaren M, Pals ST. Targeting EXT1 reveals a crucial role for heparan sulfate in the growth of multiple myeloma. Blood. 2010;115(3):601–604.

[54] Kreuger J, Spillmann D, Li J, Lindahl U. Interactions between heparan sulfate and proteins: The concept of specificity. J Cell Biol. 2006;174(3):323–327.

[55] Parish CR, Freeman C, Brown KJ, Francis DJ, Cowden WB. Identification of sulfated oligosaccharide-based inhibitors of tumor growth and metastasis using novel *in vitro* assays for angiogenesis and heparanase activity. Cancer Res. 1999;59(14):3433–3441.

[56] Yu G, Gunay NS, Linhardt RJ, Toida T, Fareed J, Hoppensteadt DA, Shadid H, Ferro V, Li C, Fewings K, Palermo MC, Podger D. Preparation and anticoagulant activity of the phosphosulfomannan PI-88. Eur J Med Chem. 2002;37(10):783–791.

[57] van Wijk XM, Thijssen VL, Lawrence R, van den Broek SA, Dona M, Naidu N, Oosterhof A, van de Westerlo EM, Kusters LJ, Khaled Y, Jokela TA, Nowak-Sliwinska P, Kremer H, Stringer SE, Griffioen AW, van Wijk E, van Delft FL, van Kuppevelt TH. Interfering with UDP-GlcNAc metabolism and heparan sulfate expression using a sugar analogue reduces angiogenesis. ACS Chem Biol. 2013;8(10):2331–2338.

[58] Weiss RJ, Gordts PL, Le D, Xu D, Esko JD, Tor Y. Small molecule antagonists of cell-surface heparan sulfate and heparin-protein interactions. Chem Sci. 2015;6(10):5984–5993.

[59] Garud DR, Tran VM, Victor XV, Koketsu M, Kuberan B. Inhibition of heparan sulfate and chondroitin sulfate proteoglycan biosynthesis. J Biol Chem. 2008;283(43):28881–28887.

[60] Umber F, Störring FK, Föllmer W. Erfolge mit einem neuartigen depot insulin ohne protaminzusatz (surfen-insulin). Klin Wochenschr. 1938;17:443–446.

[61] Roan NR, Sowinski S, Münch J, Kirchhoff F, Greene WC. Aminoquinoline surfen inhibits the action of SEVI (semen-derived enhancer of viral infection). J Biol Chem. 2010;285(3):1861–1869.

[62] Warford JR, Lamport AC, Clements DR, Malone A, Kennedy BE, Kim Y, Gujar SA, Hoskin DW, Easton AS. Surfen, a proteoglycan binding agent, reduces inflammation but inhibits remyelination in murine models of Multiple Sclerosis. Acta Neuropathol Commun. 2018;6(1):4.

[63] Lanza TJ, Durette PL, Rollins T, Siciliano S, Cianciarulo DN, Kobayashi SV, Caldwell CG, Springer MS, Hagmann WK. Substituted 4,6-diaminoquinolines as inhibitors of C5a receptor binding. J Med Chem.

1992;35(2):252–258.

[64] Panchal RG, Hermone AR, Nguyen TL, Wong TY, Schwarzenbacher R, Schmidt J, Lane D, McGrath C, Turk BE, Burnett J, Aman MJ, Little S, Sausville EA, Zaharevitz DW, Cantley LC, Liddington RC, Gussio R, Bavari S. Identification of small molecule inhibitors of anthrax lethal factor. Nat Struct Mol Biol. 2004;11(1):67–72.

[65] Hunter DT, Hill JM. Surfen: A quinoline with oncogenic and heparin-neutralizing properties. Nature. 1961;191:1378–1379.

[66] Zsila F. Glycosaminoglycan and DNA binding induced intra- and intermolecular exciton coupling of the bis-4-aminoquinoline surfen. Chirality. 2015;27(9):605–612.

[67] Passaniti A, Kleinman HK, Martin GR. Matrigel: History/background, uses, and future applications. J Cell Commun Signal. 2022;16(4):621–626.

[68] Kleinman HK, Martin GR. Matrigel: Basement membrane matrix with biological activity. Semin Cancer Biol. 2005;15(5):378–386.

[69] Hughes CS, Postovit LM, Lajoie GA. Matrigel: A complex protein mixture required for optimal growth of cell culture. Proteomics. 2010;10(9):1886–1890.

[70] Whitelock JM, Iozzo RV. Heparan sulfate: A complex polymer charged with biological activity. Chem Rev. 2005;105(7):2745–2764.

[71] Esko JD, Kimata K, Lindahl U. Proteoglycans and sulfated glycosaminoglycans. Essent Glycobiol. (2nd ed.) 2009.

[72] Sasisekharan R, Venkataraman G. Heparin and heparan sulfate: Biosynthesis, structure and function. Curr Opin Chem Biol. 2000;4(6):626–631.

[73] Sugahara K, Kitagawa H. Recent advances in the study of the biosynthesis and functions of sulfated glycosaminoglycans. Curr Opin Struct Biol. 2000;10(5):518–527.

[74] Presto J, Thuveson M, Carlsson P, Busse M, Wilén M, Eriksson I, Kusche-Gullberg M, Kjellén L. Heparan sulfate biosynthesis enzymes EXT1 and EXT2 affect NDST1 expression and heparan sulfate sulfation. Proc Natl

Acad Sci USA. 2008;105(12):4751–4756.

[75] McCormick C, Duncan G, Goutsos KT, Tufaro F. The putative tumor suppressors EXT1 and EXT2 form a stable complex that accumulates in the Golgi apparatus and catalyzes the synthesis of heparan sulfate. Proc Natl Acad Sci U S A. 2000;97(2):668-673.

[76] Lind T, Tufaro F, McCormick C, Lindahl U, Lidholt K. The putative tumor suppressors EXT1 and EXT2 are glycosyltransferases required for the biosynthesis of heparan sulfate. J Biol Chem. 1998;273(41):26265–26268.

[77] McCormick C, Leduc Y, Martindale D, Mattison K, Esford LE, Dyer AP, Tufaro F. The putative tumour suppressor EXT1 alters the expression of cell-surface heparan sulfate. Nat Genet. 1998;19(2):158-161.

[78] Leisico F, Omeiri J, Le Narvor C, Beaudouin J, Hons M, Fenel D, Schoehn G, Couté Y, Bonnaffé D, Sadir R, Lortat-Jacob H, Wild R. Structure of the human heparan sulfate polymerase complex EXT1-EXT2. Nat Commun. 2022;13(1):7110.

[79] Kinoshita T, Tomita H, Okada H, Niwa A, Hyodo F, Kanayama T, Matsuo M, Imaizumi Y, Kuroda T, Hatano Y, Miyai M, Egashira Y, Enomoto Y, Nakayama N, Sugie S, Matsumoto K, Yamaguchi Y, Matsuo M, Hara H, Iwama T, Hara A. Endothelial cell-specific reduction of heparan sulfate suppresses glioma growth in mice. Discov Oncol. 2021;12(1):50.

[80] Okada M, Nadanaka S, Shoji N, Tamura J, Kitagawa H. Biosynthesis of heparan sulfate in *EXT1*-deficient cells. Biochem J. 2010;428(3):463–471.

[81] Chen J, Wang Y, Chen C, Lian C, Zhou T, Gao B, Wu Z, Xu C. Exogenous Heparan Sulfate Enhances the TGF-β3-Induced Chondrogenesis in Human Mesenchymal Stem Cells by Activating TGF-β/Smad Signaling. Stem Cells Int. 2016;2016:1520136.

[82] Gaus S, Li H, Li S, Wang Q, Kottek T, Hahnel S, Liu X, Deng Y, Ziebolz D, Haak R, Schmalz G, Liu L, Savkovic V, Lethaus B. Shared Genetic and Epigenetic Mechanisms between the Osteogenic Differentiation of Dental Pulp Stem Cells and Bone Marrow Stem Cells. Biomed Res Int. 2021;2021:6697810.

[83] Yu J, He H, Tang C, Zhang G, Li Y, Wang R, Shi J, Jin Y. Differentiation

potential of STRO-1+ dental pulp stem cells changes during cell passaging. BMC Cell Biol. 2010;11:32.

[84] Nagase H, Visse R, Murphy G. Structure and function of matrix metalloproteinases and TIMPs. Cardiovasc Res. 2006;69(3):562–573.

[85] Yu WH, Woessner JF. Heparan sulfate proteoglycans as extracellular docking molecules for matrilysin (matrix metalloproteinase 7). J Biol Chem. 2000;275(6):4183–4191.

[86] Agere SA, Akhtar N, Watson JM, Ahmed S. RANTES/CCL5 induces collagen degradation by activating MMP-1 and MMP-13 expression in human rheumatoid arthritis synovial fibroblasts. Front Immunol. 2017;8:1341.

[87] Pfeifer V, Weber H, Wang Y, Schlesinger M, Gorzelanny C, Bendas G. Exostosin 1 knockdown induces chemoresistance in MV3 melanoma cells by upregulating JNK and MEK/ERK signaling. Int J Mol Sci. 2023;24(6):5452.

[88] Wang X, Cornelis FMF, Lories RJ, Monteagudo S. Exostosin-1 enhances canonical Wnt signaling activity during chondrogenic differentiation. Osteoarthritis Cartilage. 2019;27(11):1702–1710.

[89] Sakai VT, Cordeiro MM, Dong Z, Zhang Z, Zeitlin BD, Nör JE. Tooth slice/scaffold model of dental pulp tissue engineering. Adv Dent Res. 2011;23(3):325–332.

[90] Sakai VT, Zhang Z, Dong Z, Neiva KG, Machado MA, Shi S, Santos CF, Nör JE. SHED differentiate into functional odontoblasts and endothelium. J Dent Res. 2010;89(8):791-796.

[91] Rosa V, Zhang Z, Grande RH, Nör JE. Dental pulp tissue engineering in full-length human root canals. J Dent Res. 2013;92(11):970-975.

[92] Gonçalves SB, Dong Z, Bramante CM, Holland GR, Smith AJ, Nör JE. Tooth slice–based models for the study of human dental pulp angiogenesis. J Endod. 2007;33(7):811–814.

[93] Mullane EM, Dong Z, Sedgley CM, Hu JC, Botero TM, Holland GR, Nör JE. Effects of VEGF and FGF2 on the revascularization of severed human dental pulps. J Dent Res. 2008;87(12):1144-1148.

[94] Cordeiro MM, Dong Z, Kaneko T, Zhang Z, Miyazawa M, Shi S, Smith AJ,

Nör JE. Dental pulp tissue engineering with stem cells from exfoliated deciduous teeth. J Endod. 2008;34(8):962-969.

[95] Batouli S, Miura M, Brahim J, Tsutsui TW, Fisher LW, Gronthos S, Robey PG, Shi S. Comparison of stem-cell-mediated osteogenesis and dentinogenesis. J Dent Res. 2003;82(12):976-981.

[96] Yang J, Motlagh D, Allen JB, Webb AR, Kibbe MR, Aalami O, Kapadia M, Carroll TJ, Ameer GA. Modulating expanded polytetrafluoroethylene vascular graft host response via citric acid-based biodegradable elastomers. Adv Mater. 2006;18(12):1493–1498.

[97] Gentile P, Chiono V, Tonda-Turo C, Ferreira AM, Ciardelli G. Polymeric membranes for guided bone regeneration. Biotechnol J. 2011;6(10):1187–1197.

Figures and tables

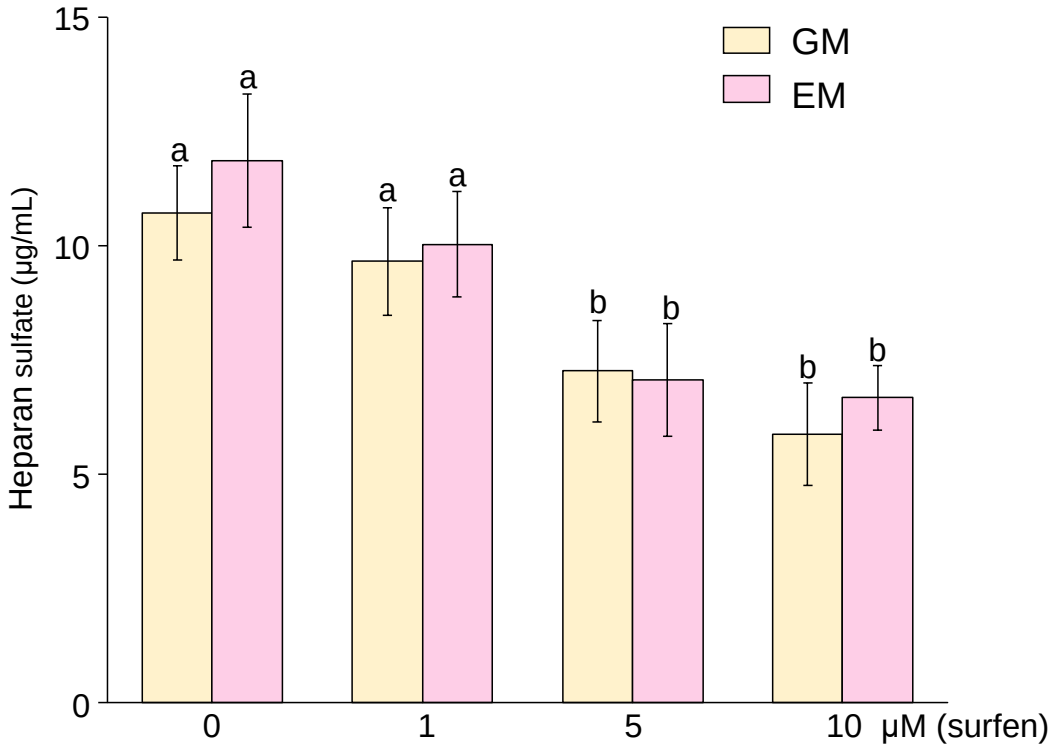

Figure 1. HS production under GM or EM induction with surfen stimulation.

HS: heparan sulfate; GM: growth medium; EM: endothelial differentiation medium. Different letters indicate significant differences among groups. *P < 0.05, ANOVA and Tukey's HSD test, n = 4.

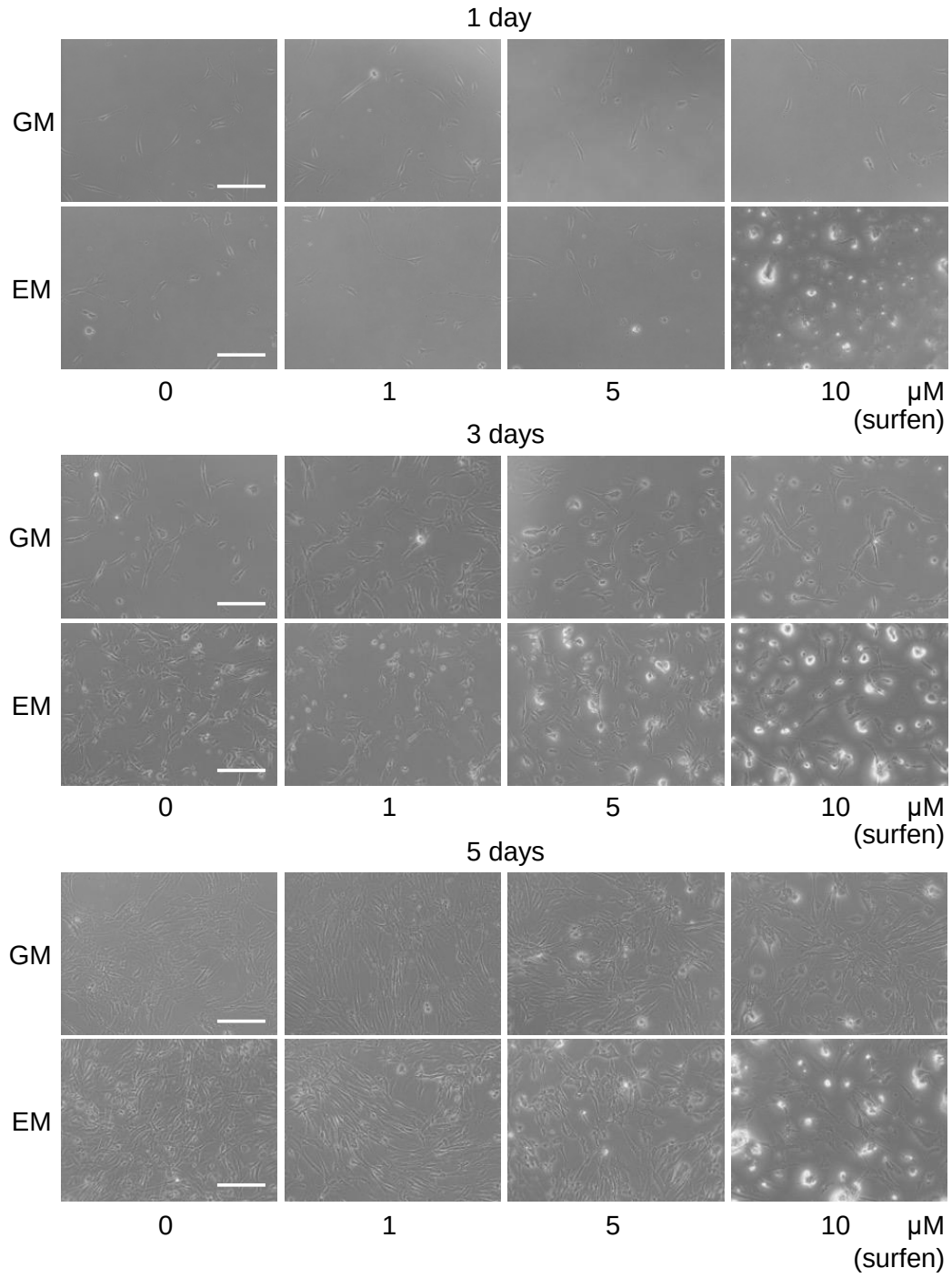

Figure 2. Photomicrographs of DPSCs grown in GM or EM containing surfen.

Scale bars: 200 μm.

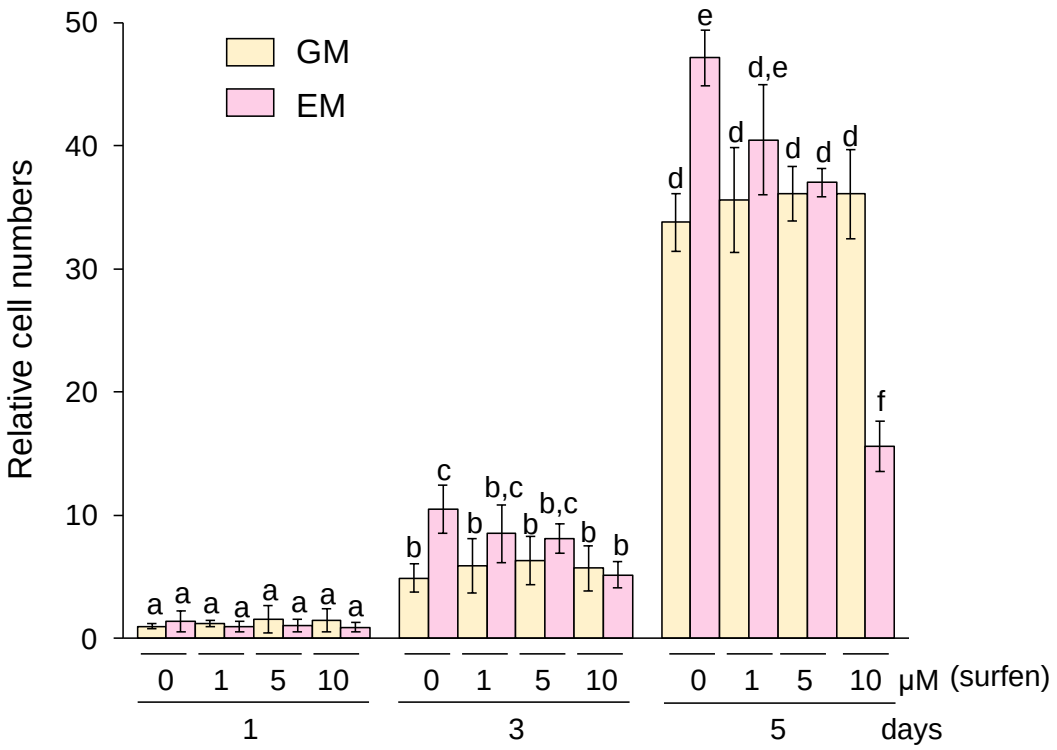

Figure 3. DPSCs proliferation in the presence of GM or EM containing surfen.

Different letters indicate significant differences among groups. *$P < 0.05$, ANOVA and Tukey's HSD test, $n = 4$.

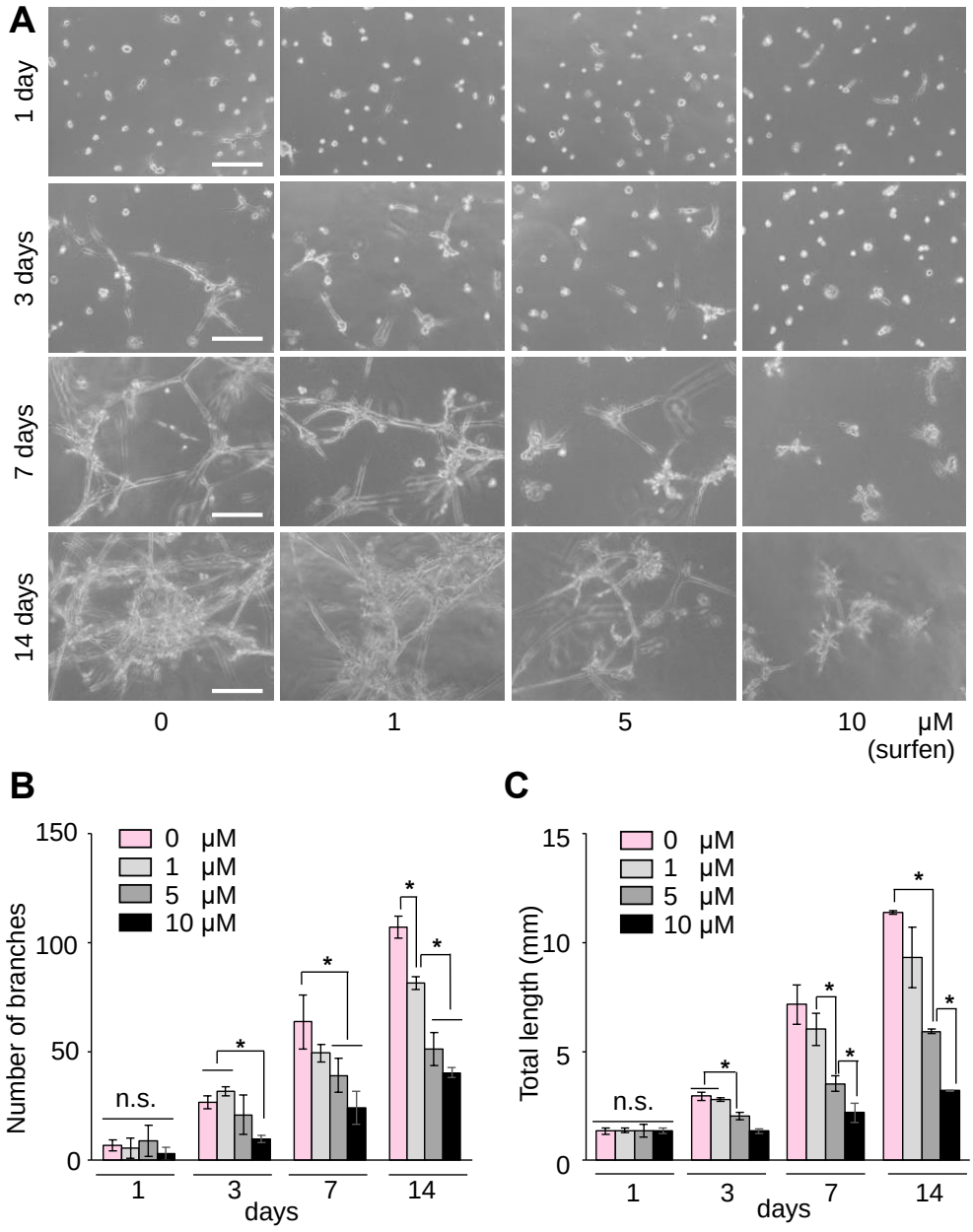

Figure 4. Sprouting behaviors of DPSCs under exposure to surfen.

(A) Representative bright-field images of DPSCs with sprouting formations induced by EM containing 1, 5, or 10 μM surfen. Scale bars: 200 μm. (B, C) Quantification of numbers of branches and total lengths of sprouts at corresponding time points. n.s., no significant difference. *$P < 0.05$, ANOVA and Tukey's HSD test, $n = 4$.

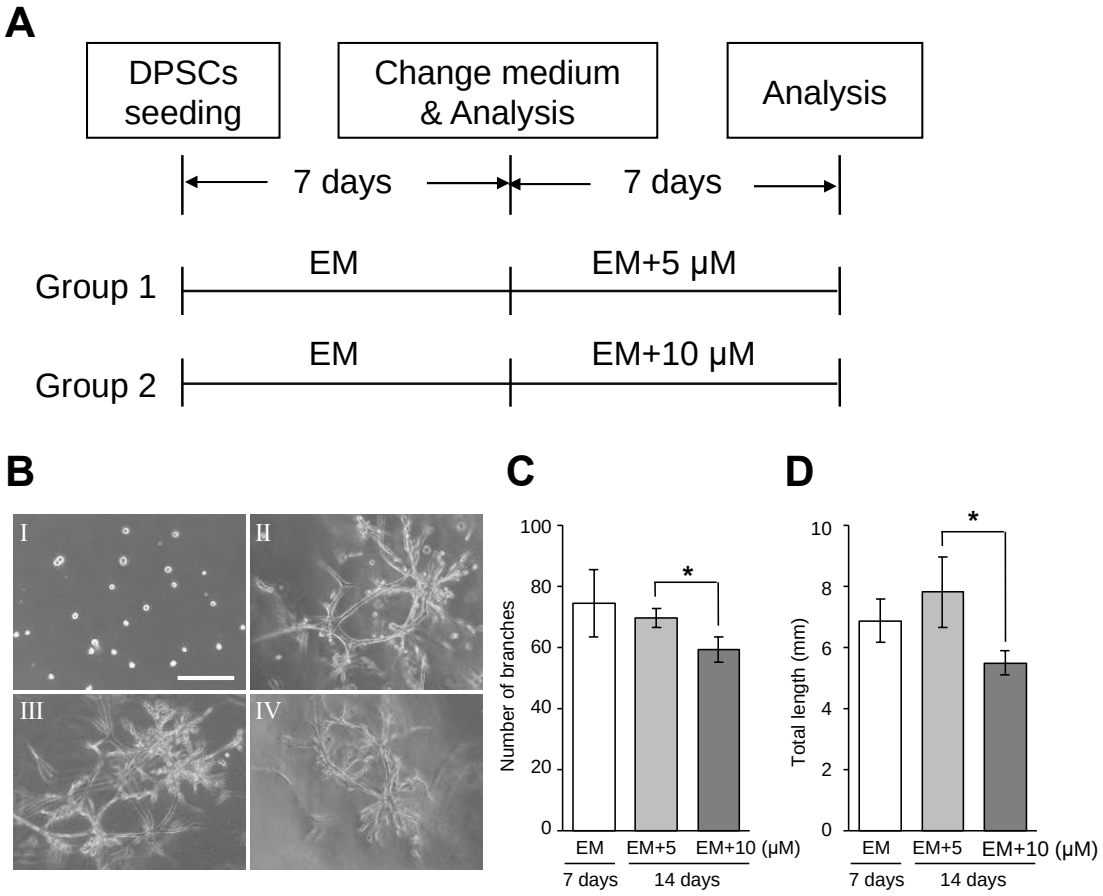

Figure 5. Devitalization of the sprouting ability of DPSCs.

(A) Experimental design for sprouting devitalization and detailed group information. (B) Photomicrographs of DPSCs seeded onto Matrigel at day 0 (I) and maintained in endothelial differentiation medium (EM) for the first 7 days (II). Photomicrographs of DPSCs cultured with EM containing 5 and 10 μM surfen for another 7 days were depicted in (III) and (IV). (C, D) Quantification of numbers of branches and total lengths for both groups after 14 days of culture. Scale bar: 200 μm. *$P < 0.05$, ANOVA and Tukey's HSD test, $n = 4$.

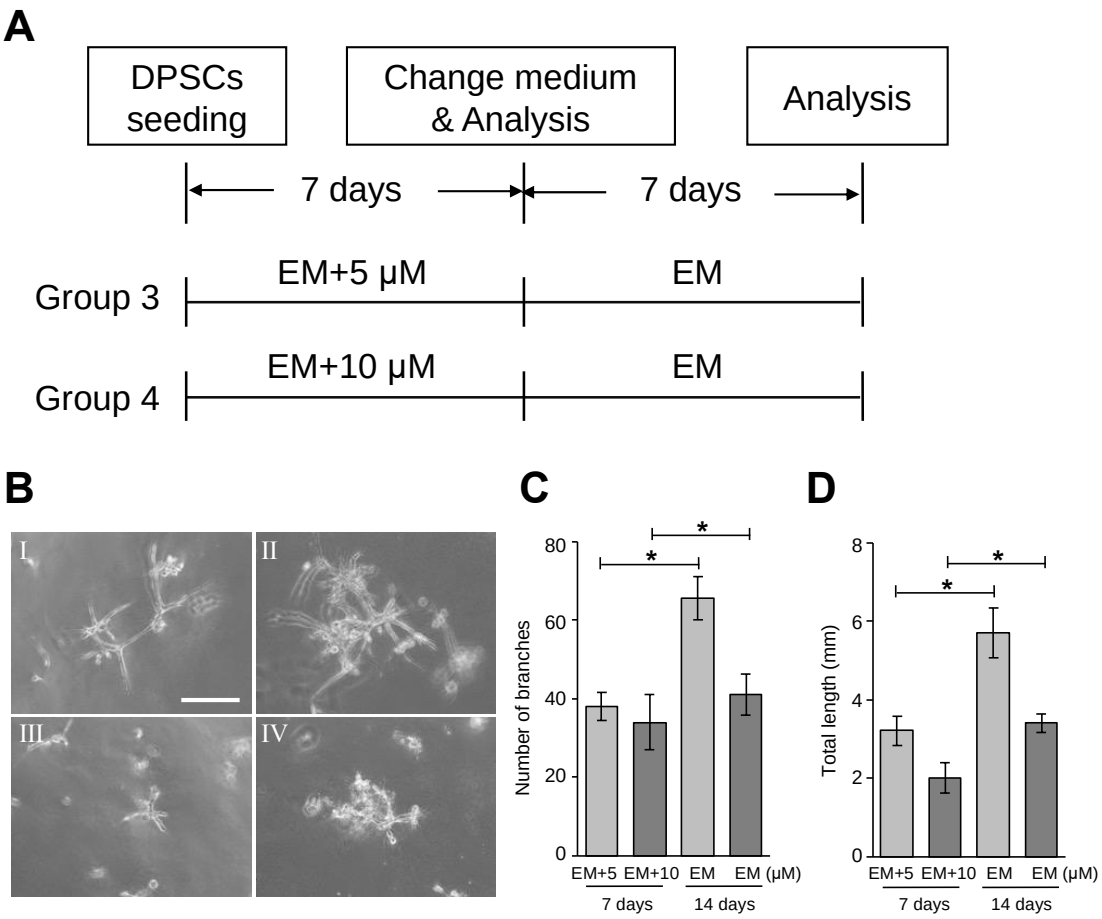

Figure 6. Revitalization of the sprouting ability of DPSCs.

(A) Experimental design for sprouting revitalization. (B) Photomicrographs of DPSCs cultured with EM containing 5 μM surfen for the first 7 days (I) and then maintained in EM without surfen for another 7 days (II). Photomicrographs of DPSCs cultured with EM containing 10 μM surfen for the first 7 days (III) and then maintained in EM without surfen for another 7 days (IV). (C, D) Quantification of number of branches and total length for both groups after 14 days of culture. Scale bars: 200 μm. *P < 0.05, ANOVA and Tukey's HSD test, n = 4.

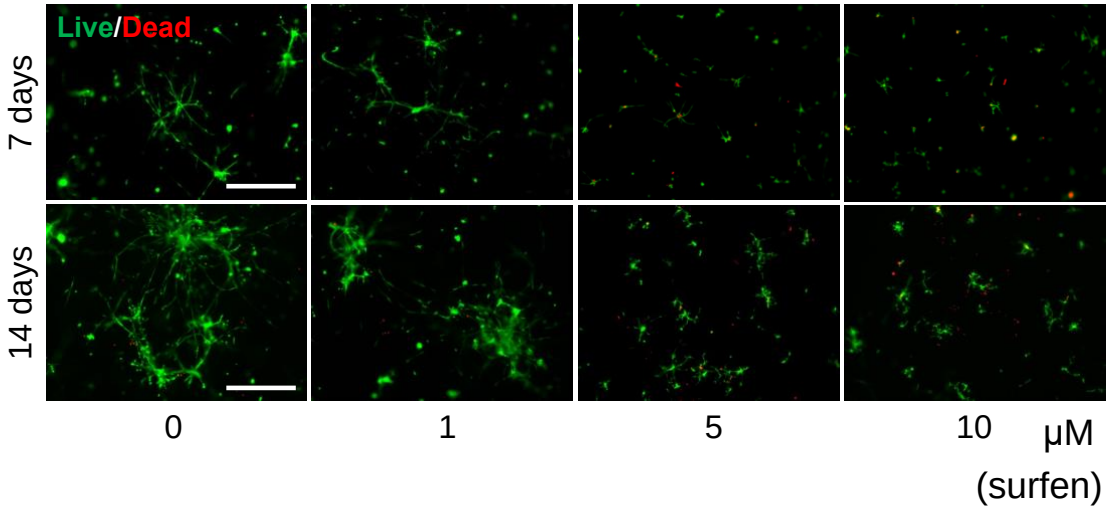

Figure 7. Viability of DPSCs under endothelial induction with surfen.

Live and dead cells were stained with green and red color, respectively. Scale bars: 500 μm.

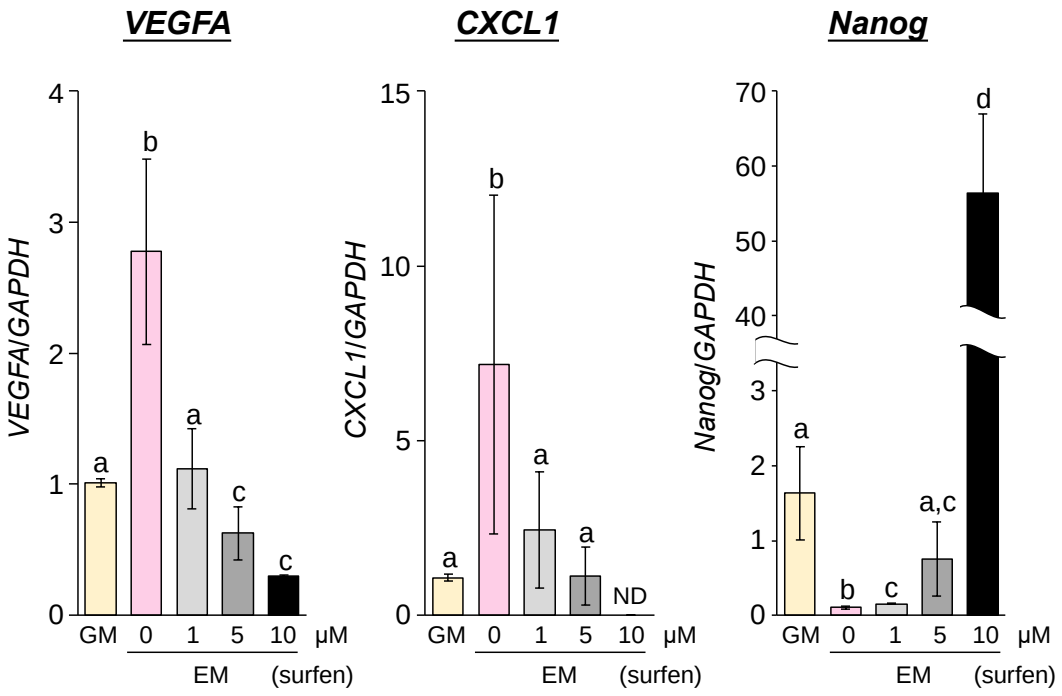

Figure 8. Endothelial and stemness-related gene expression in DPSCs cultured with GM or surfen-containing EM.

Gene expressions of *vascular endothelial growth factor A* (*VEGFA*), *C-X-C motif chemokine ligand 1* (*CXCL1*), and *Nanog* after 7 days of incubation were evaluated by real-time PCR. Expression of *glyceraldehyde 3-phosphate dehydrogenase* (*GAPDH*) was used as a reference gene. One of the GM replicates was used to normalize all samples. Different letters indicate significant differences among groups. ND, not detected. *$P < 0.05$, ANOVA and Tukey's HSD test, $n = 4$.

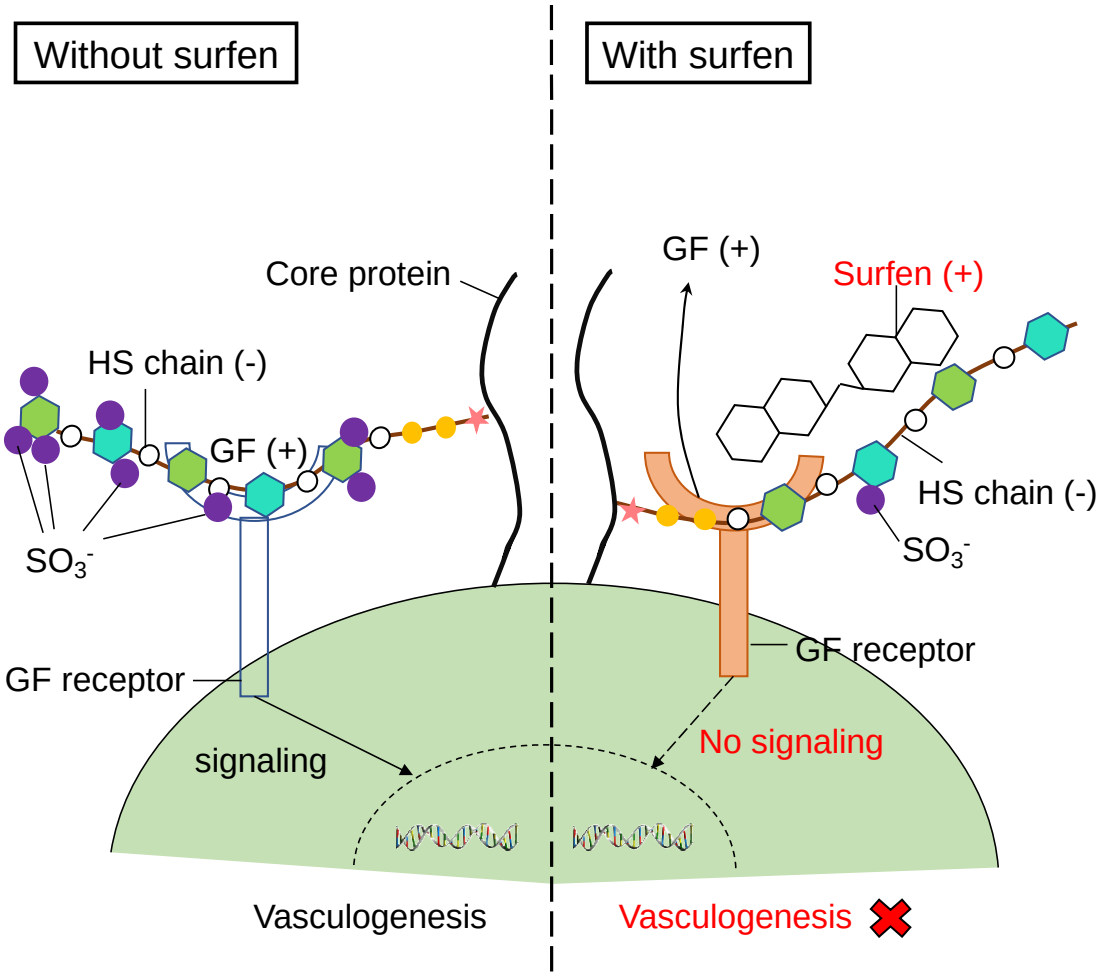

Figure 9. Possible mechanism of the suppressed vasculogenesis of DPSCs by surfen stimulation.

Surfen binds to HS by electronic interaction, which interferes the combination between HS and growth factors (GFs), subsequently inhibiting cellular activities dependent on HS, including vasculogenesis.

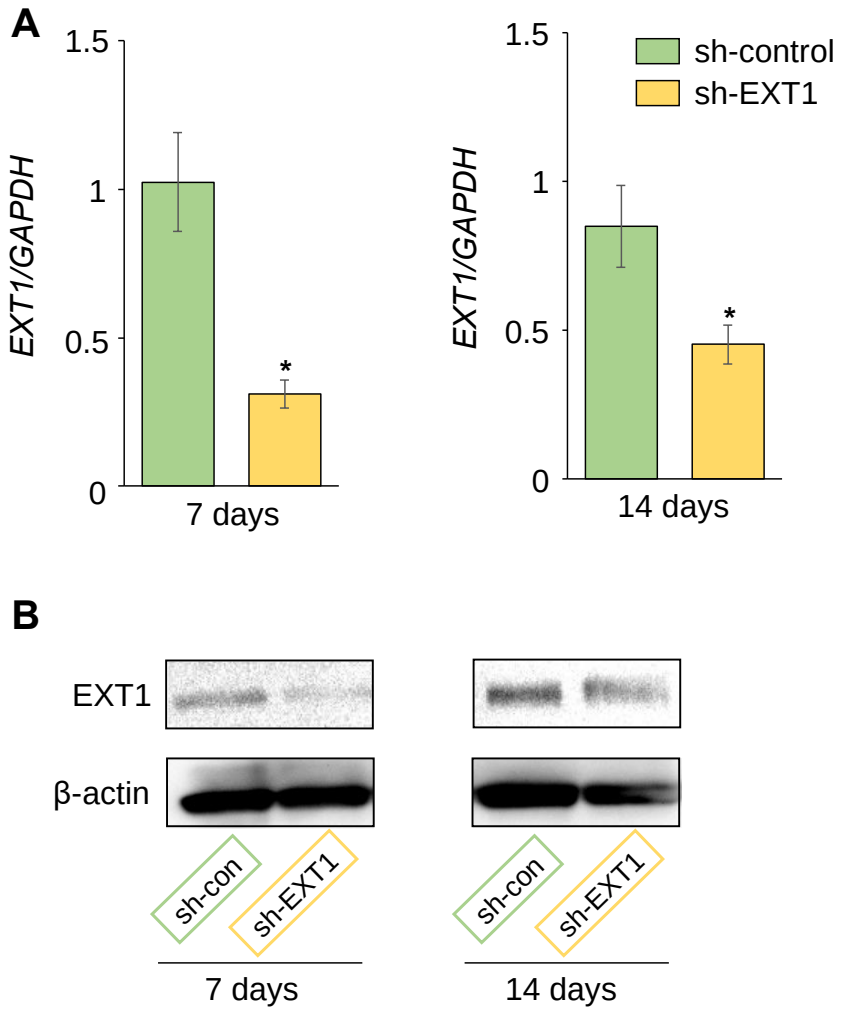

Figure 10. EXT1 expressions in *EXT1*-silenced (sh-EXT1) and sh-control DPSCs.

The mRNA and protein levels of EXT1 were evaluated by real-time PCR (A) and western blotting assay (B), respectively. sh-control: scrambled sequence-transduced DPSCs. *$P < 0.05$, Student's *t*-test, $n = 4$.

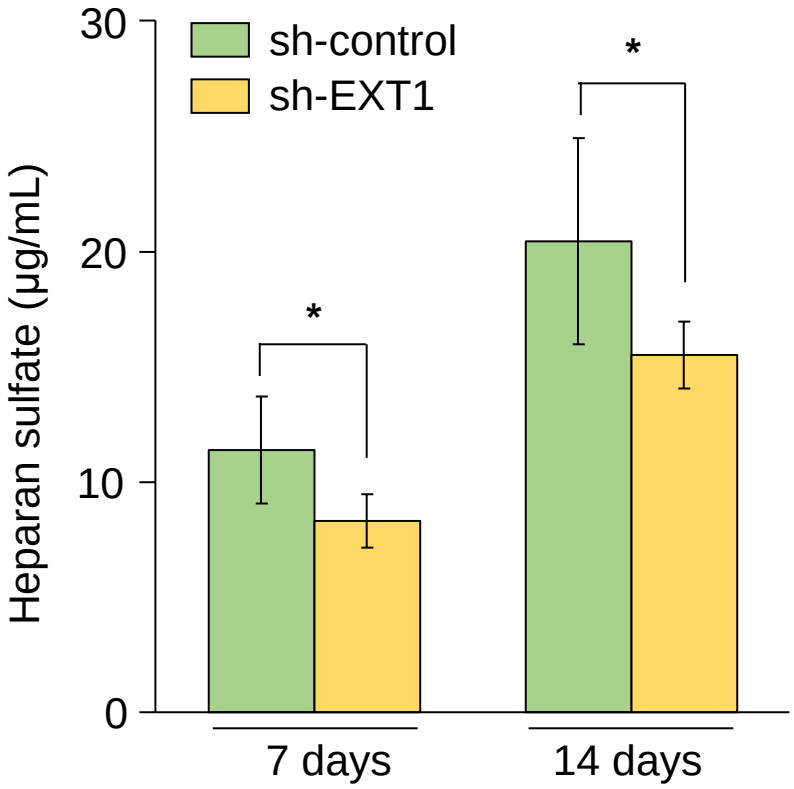

Figure 11. HS production after *EXT1* silencing in DPSCs.

sh-EXT1: *EXT1*-silenced DPSCs; sh-control: scrambled sequence-transduced DPSCs. *$P < 0.05$, Student's *t*-test, $n = 4$.

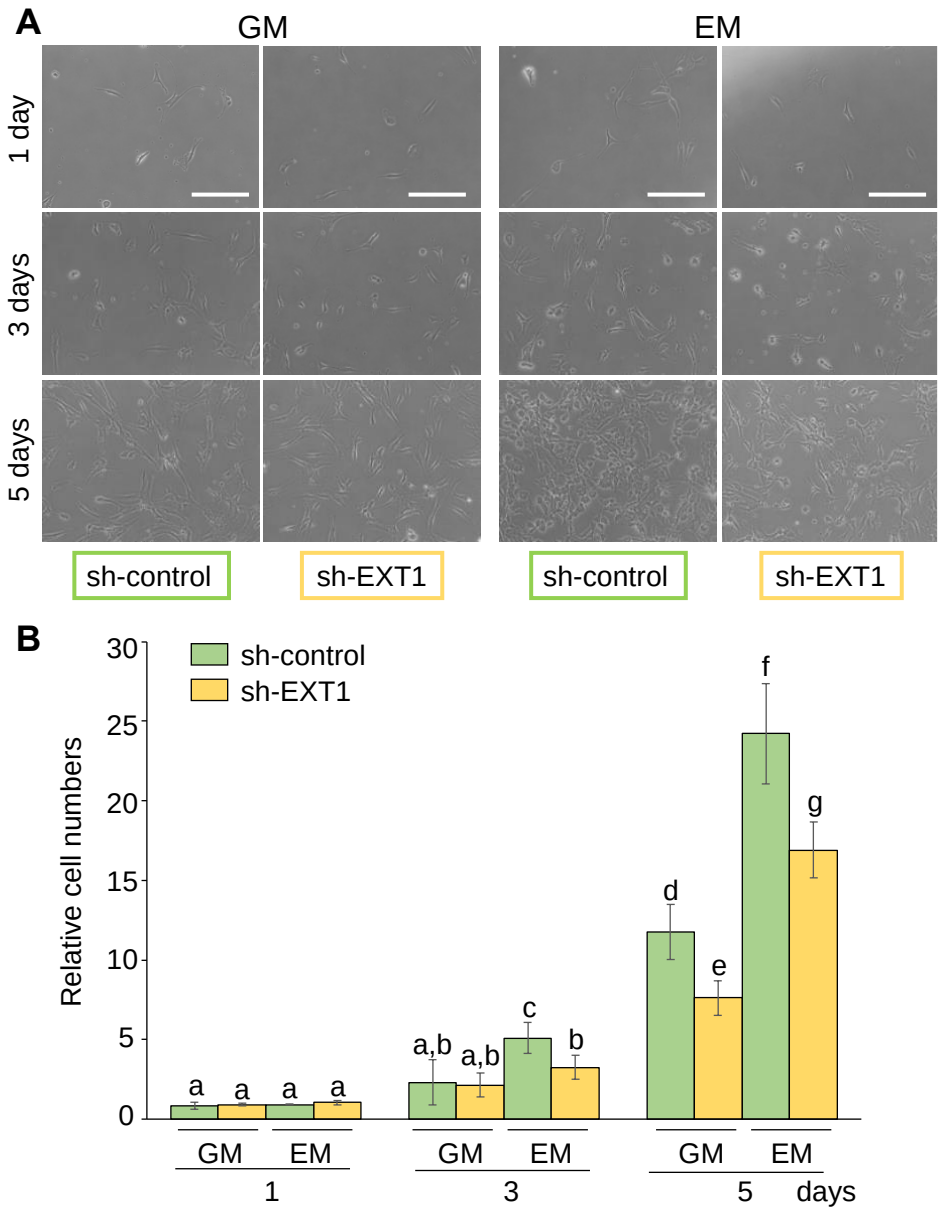

Figure 12. Proliferation of *EXT1*-silenced (sh-EXT1) and sh-control DPSCs *in vitro*.

(A) Photomicrographs of DPSCs cultured with sh-EXT1 or sh-control in GM or EM for 5 days. (B) Graph depicting cell numbers of sh-EXT1 and sh-control DPSCs at 1, 3, and 5 days. Different letters represent significant differences among groups. Scale bars: 200 μm. *$P < 0.05$, ANOVA and Tukey's HSD test, $n = 4$.

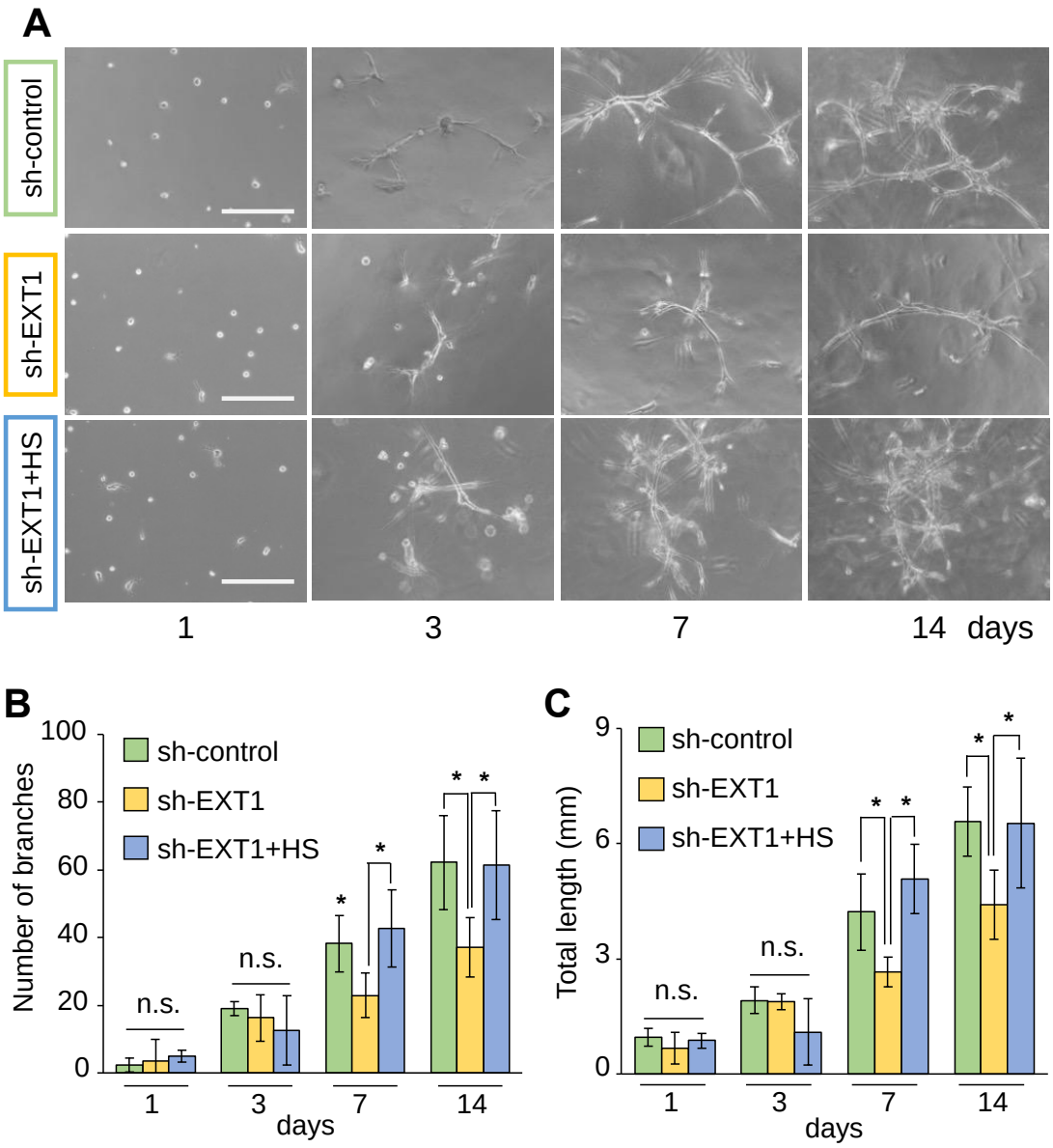

Figure 13. Sprouting ability of *EXT1*-silenced (sh-EXT1) DPSCs with exogenous HS.

(A) Representative bright-field images of capillary spouts of DPSCs cultured with sh-control, sh-EXT1, or sh-EXT1 supplemented with 100 μg/ml of HS (sh-EXT1+HS). Scale bars: 200 μm. (B,C) Quantification of numbers of branches and total length of sprouts at indicated time points. *$P < 0.05$, ANOVA and Tukey's HSD test, $n = 5$.

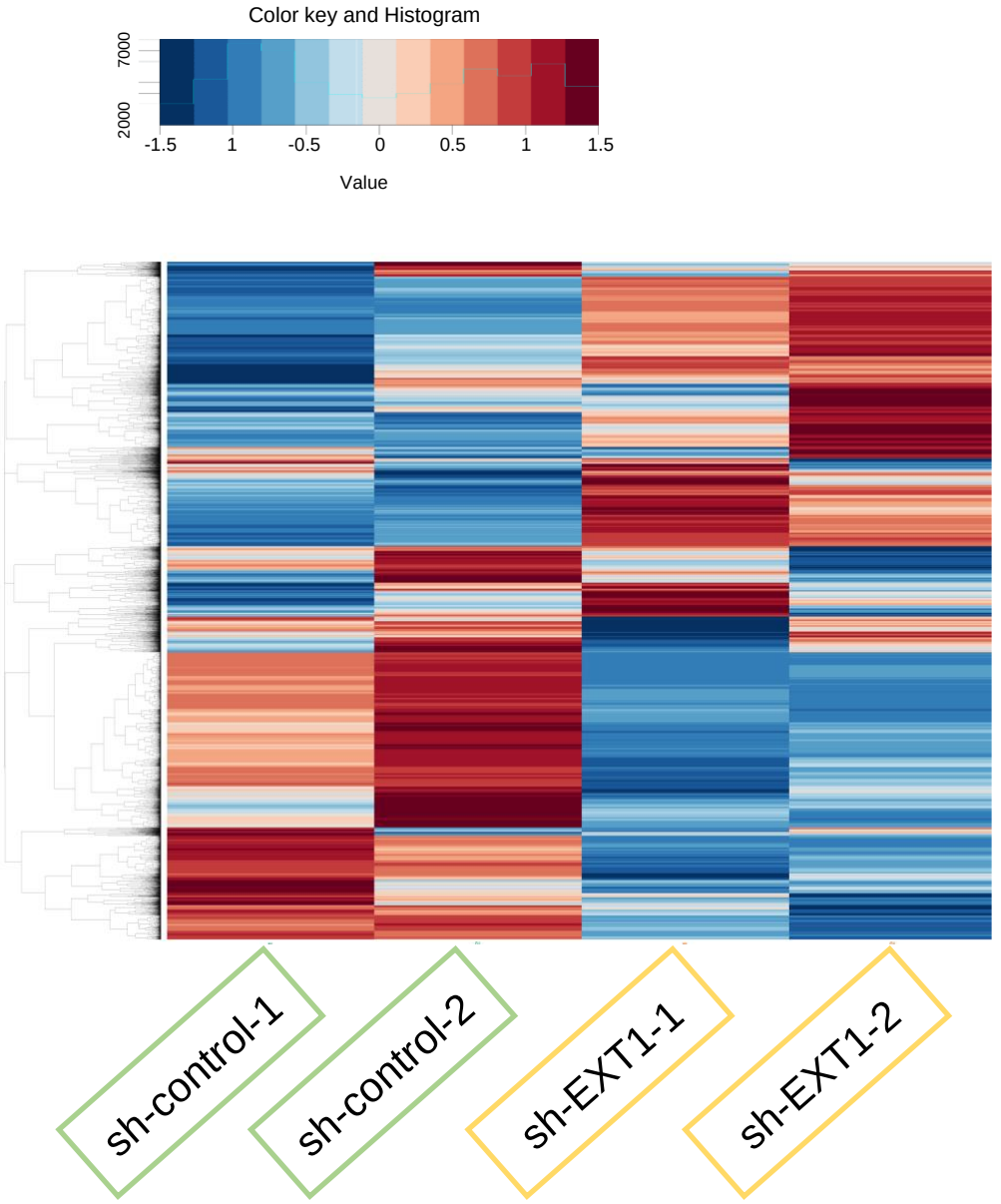

Figure 14. Hierarchical clustering heatmap after silencing *EXT1* in DPSCs.

Heatmap displays standardized gene expression values ranging from -1.5 to 1.5 with a mean of 0 for sh-EXT1 and sh-control. Red color represents genes with high expression levels, whereas blue color indicates genes with low expression levels. sh-EXT1: *EXT1*-silenced DPSCs; sh-control: scrambled sequence-transduced DPSCs.

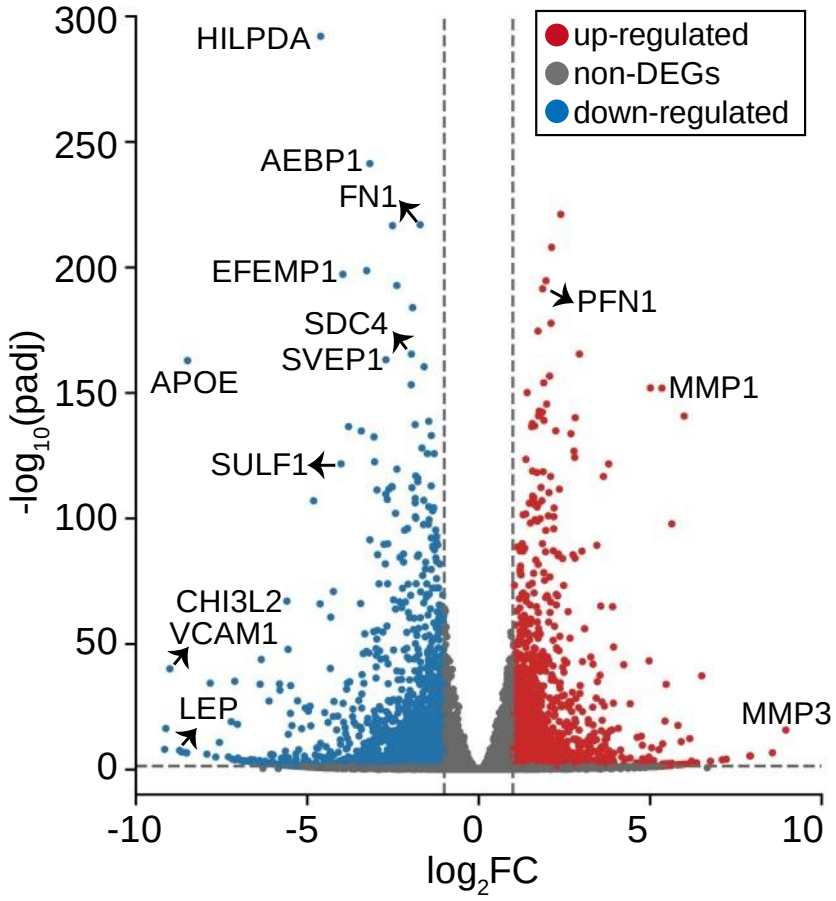

Figure 15. Volcano plot visualization of genes upregulated or downregulated in *EXT1*-silenced DPSCs.

Gene values with $|\log_2 FC| > 1$ and p adj < 0.05 were considered differentially expressed genes (DEGs). Red dots represent upregulated genes, while blue dots represent downregulated genes. Gray represents non-significant DEGs (non-DEGs).

Table 1. List of downregulated genes from DEG analysis (sh-EXT1/sh-control).

DEG: differentially expressed genes. sh-EXT1: *EXT1*-silenced DPSCs; sh-control: scrambled sequence-transduced DPSCs.

Symbol	Full name	Gene ID	Fold change	P adjust
ACVRL1	Activin A Receptor Like Type 1	ENSG00000139567	0.323466047	3.37E-05
APOE	Apolipoprotein	ENSG00000130203	0.002788866	1.62E-163
CCL2	C-C Motif Chemokine Ligand 2	ENSG00000108691	0.20221355	1.73E-08
CXCL1	Chemokine (C-X-C motif) Ligand 1	ENSG00000163739	0.175588416	0.012385732
CXCL8	Chemokine (C-X-C motif) Ligand 8	ENSG00000169429	0.017468381	6.93239E-06
CYP1B1	Cytochrome P450 1B1	ENSG00000138061	0.153179096	1.73772E-74
EFNA1	Ephrin A1	ENSG00000169242	0.240782923	0.002105027
EGR3	Early Growth Response Protein 3	ENSG00000179388	0.012084205	0.004840124
ENPEP	Glutamyl Aminopeptidase	ENSG00000138792	0.137617766	3.29264E-08
ENPP2	Ectonucleotide Pyrophosphatase/Phosphodiesterase 2	ENSG00000136960	0.191139471	4.05562E-20
EPHB4	Ephrin Type-B Receptor 4	ENSG00000196411	0.138317753	9.02E-23
EXT1	Exostosin 1	ENSG00000182197	0.354570305	6.63189E-34
HIF3A	Hypoxia Inducible Factor 3 Subunit Alpha	ENSG00000124440	0.389412554	0.000146836
LEP	Leptin	ENSG00000174697	0.306880265	2.98764E-08
LEPR	Leptin Receptor	ENSG00000116678	0.007286223	1.98001E-67
MMRN2	Multimerin 2	ENSG00000173269	0.002373975	0.00619099
NOS3	Nitric Oxide Synthase 3	ENSG00000164867	0.202244431	0.005024969
PLCD1	Phospholipase C Delta 1	ENSG00000187091	0.048116378	1.77449E-10
PLXDC1	Plexin Domain Containing 1	ENSG00000161381	0.097335651	0.006481624
PLXND1	Plexin D1	ENSG00000004399	0.099315275	1.53946E-46
PRKX	Protein Kinase X-Linked	ENSG00000183943	0.126540581	1.63479E-07
PTEN	Phosphatase and Tensin Homolog	ENSG00000171862	0.425982243	4.72476E-44
TGFβ1	Transforming Growth Factor β 1	ENSG00000120708	0.479778591	2.86981E-52
TMEM100	Transmembrane Protein 100	ENSG00000166292	0.148238098	0.001471164
TYMP	Thymidine Phosphorylase	ENSG00000025708	0.299123152	0.008552182
VASH1	Vasohibin 1	ENSG00000071246	0.410622842	2.28376E-09
VCAM1	Vascular Cell Adhesion Protein 1	ENSG00000162692	0.40803335	9.44447E-41
VEGFA	Vascular Endothelial Growth Factor A	ENSG00000112715	0.179172096	1.56914E-41
VEGFB	Vascular Endothelial Growth Factor B	ENSG00000173511	0.039145952	3.0764E-18

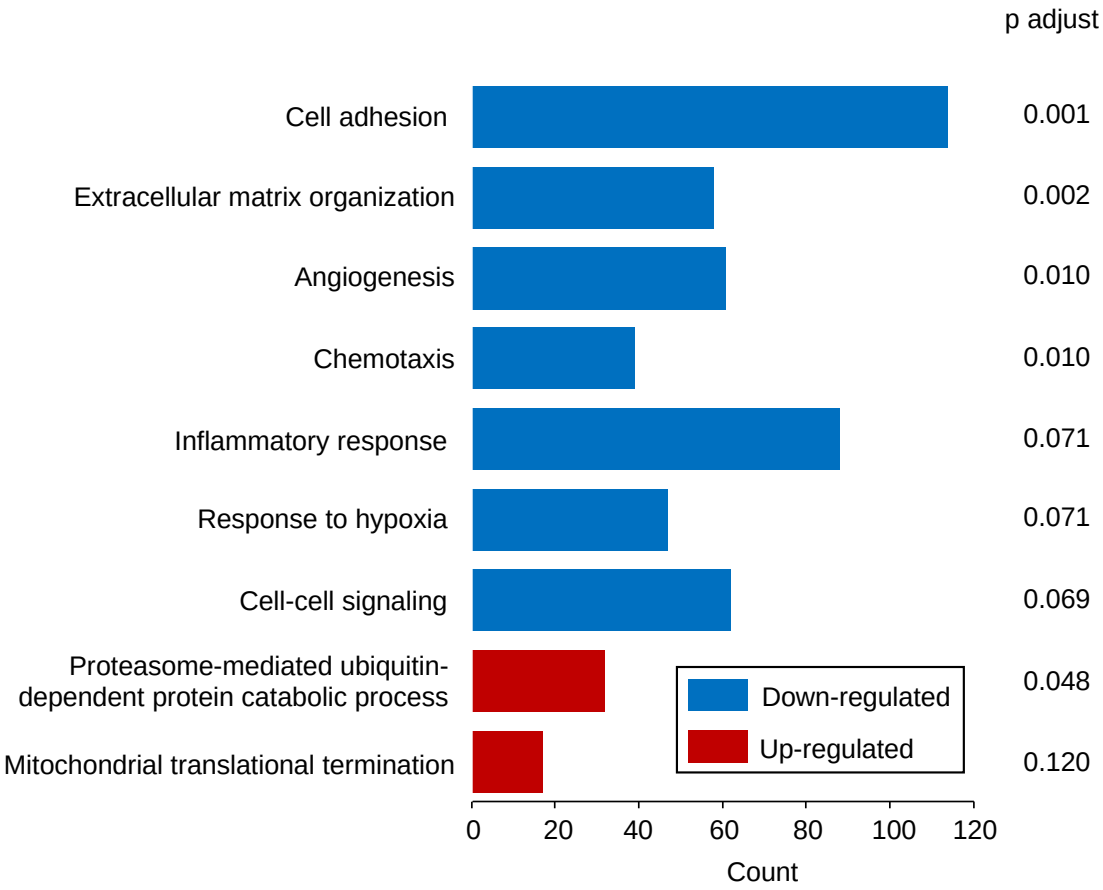

Figure 16. GO enrichment analysis of DEGs related to angiogenic or HS-associated biological processes in *EXT1*-silenced DPSCs.

Red column represents upregulated genes, while blue column represents downregulated genes. GO: gene ontology; DEGs: differentially expressed genes.

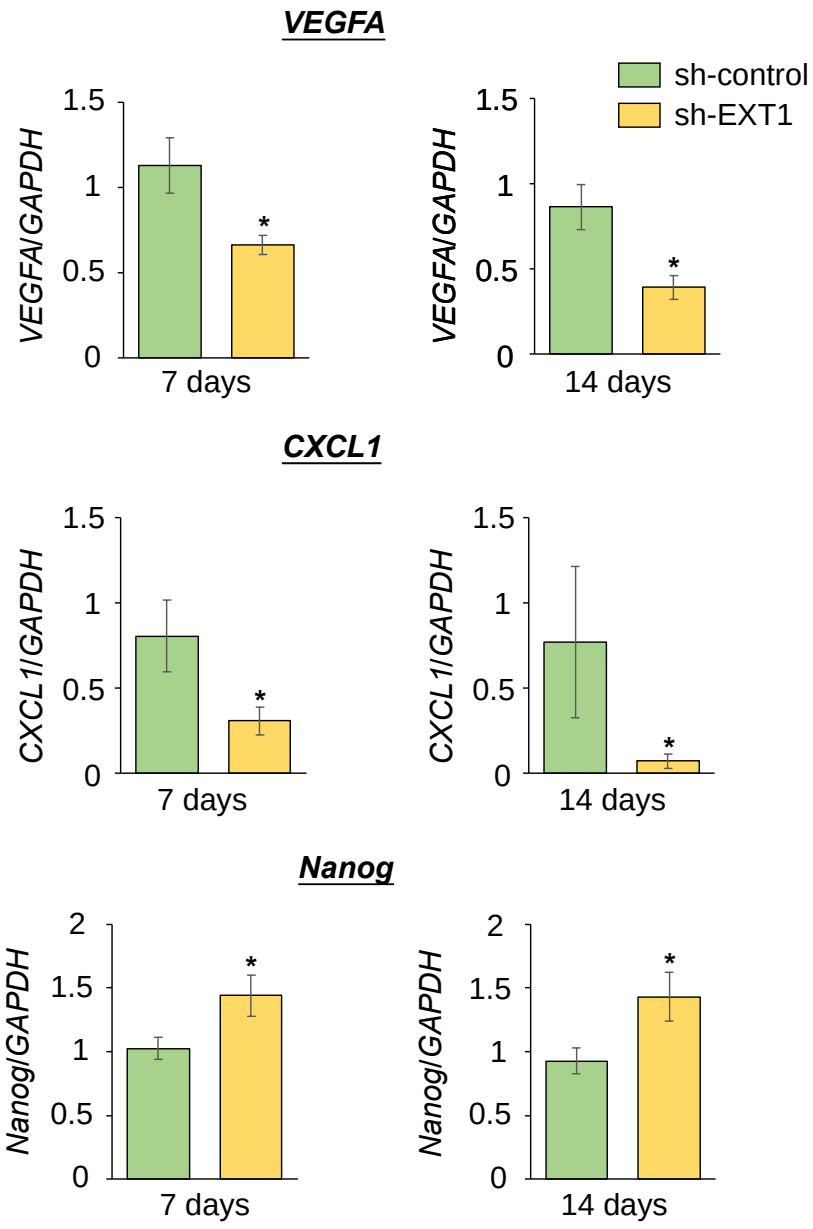

Figure 17. Gene expressions of endothelial differentiation and stemness-related marker in the *EXT1*-silenced (sh-EXT1) and sh-control DPSCs. Expression of *VEGFA*, *CXCL1*, and *Nanog* after 7 and 14 days of differentiation was determined by real-time PCR**.** The expression of *GAPDH* was used as an internal control. **P* < 0.05, Student's *t*-test, *n* = 4.

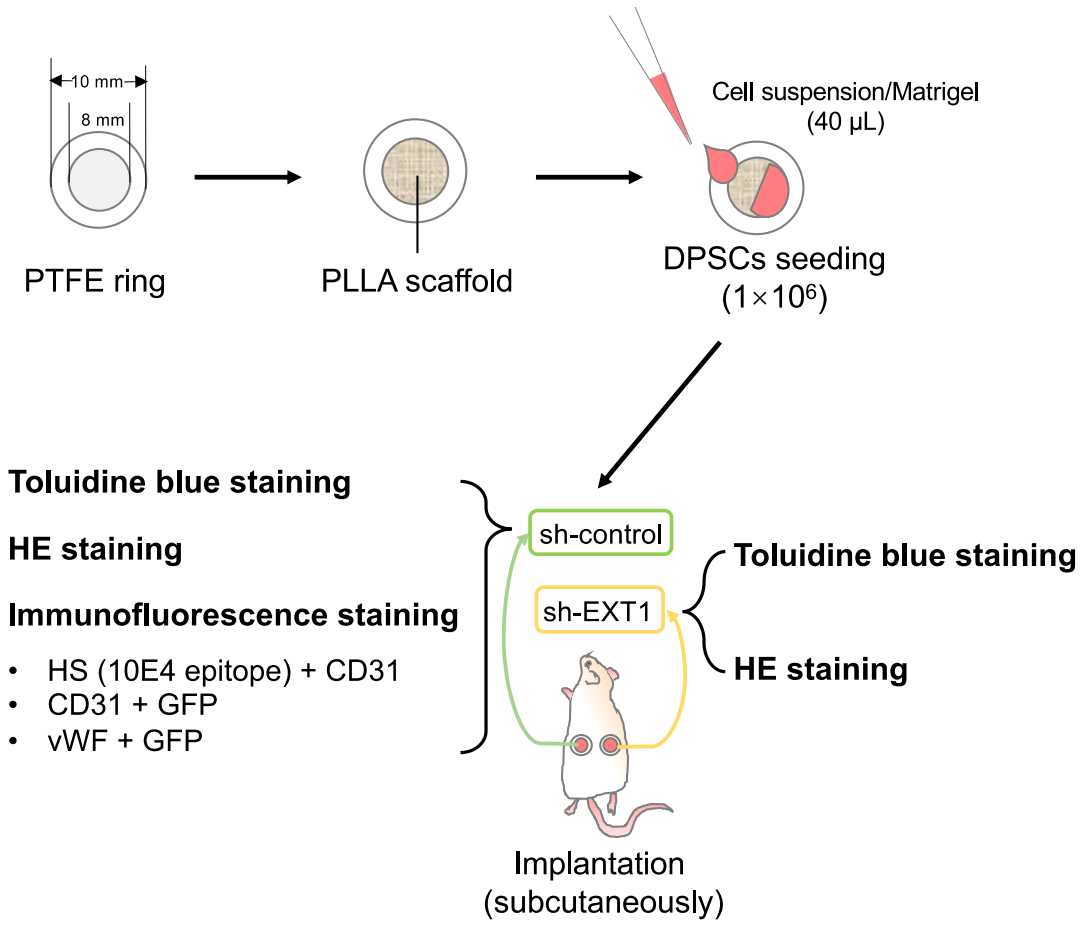

Figure 18. Fabrication of PLLA scaffold and implantation into the immunodeficient mice model.

PTFE: polytetrafluoroethylene; PLLA: poly-L-lactide acid; sh-EXT1: *EXT1*-silenced DPSCs; sh-control: scrambled sequence-transduced DPSCs; GFP: green fluorescent protein; vWF: von Willebrand factor.

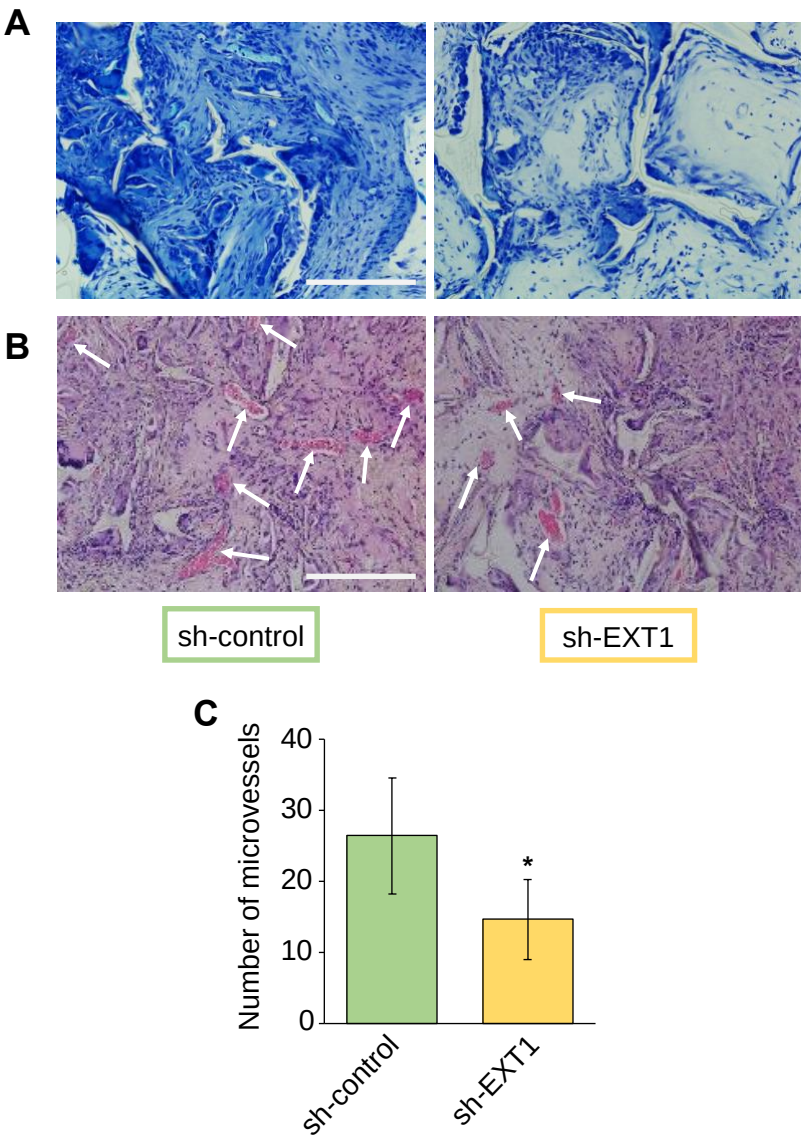

Figure 19. Polysaccharide and blood-containing vessels formed by *EXT1*-silenced DPSCs *in vivo*.

(A) Toluidine blue staining and (B) hematoxylin and eosin (HE) staining of the specimen loaded with sh-control and sh-EXT1 DPSCs. White arrows indicate blood-containing vessels. Scale bars: 200 μm. (C) Quantitative analysis of blood-containing vessels formed within the scaffolds. *$P < 0.05$, Student's *t*-test, $n = 5$.

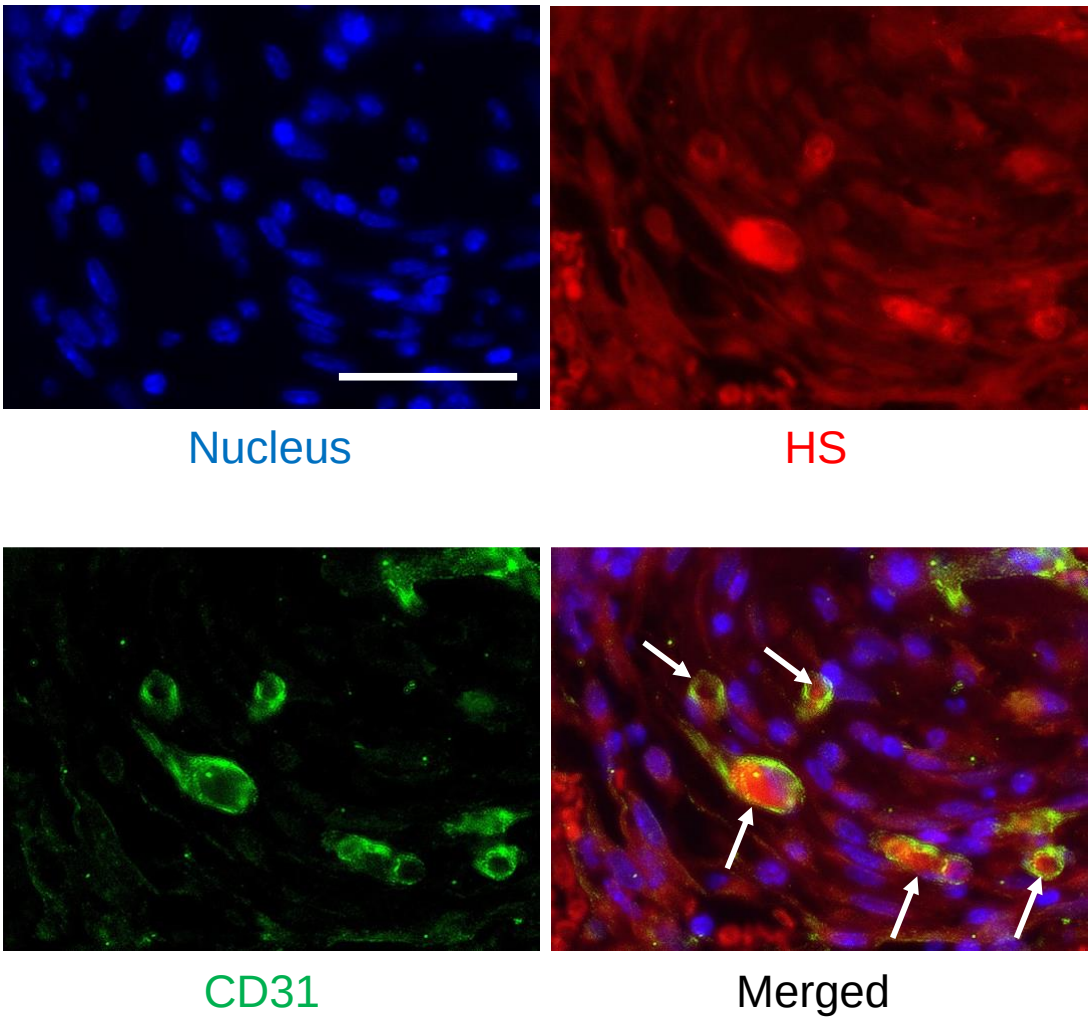

Figure 20. HS and CD31 expressions in the specimen loaded with GFP-transduced DPSCs.

White arrows indicate CD31-positive lumen-like structures supported by HS.

Scale bar: 20 μm.

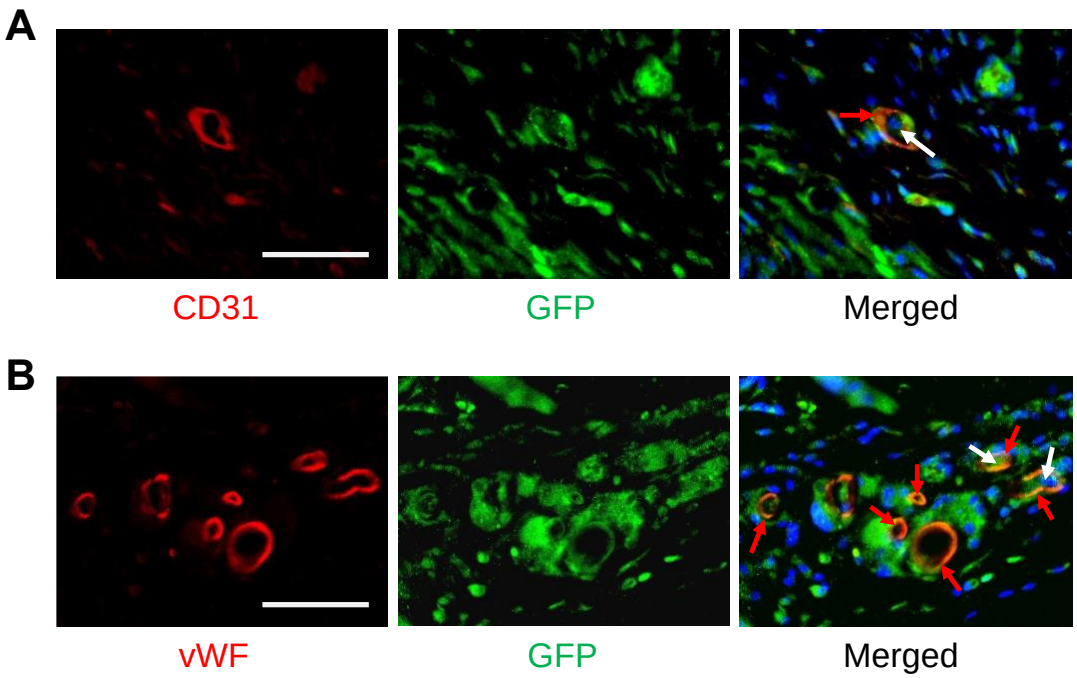

Figure 21. Vasculogenesis of GFP-transduced DPSCs *in vivo.*

Immunofluorescence staining of microvessels positive for (A) CD31 or (B) von Willebrand factor (vWF), and GFP-positive DPSCs. Cell nuclei are stained in blue. Red arrows indicate CD31 or vWF-positive lumen-like structures originating from GFP-transduced DPSCs. White arrows indicate circulating blood cells inside microvessels formed by DPSCs. Scale bars: 20 μm.